



1 High seasonal and spatial dynamics of bio- and photodegradation  
2 in boreal humic waters

3

4 Artem V. Chupakov<sup>1</sup>, Anna A. Chupakova<sup>1</sup>, Svetlana A. Zabelina<sup>1</sup>,

5 Liudmila S. Shirokova<sup>1,2</sup>, Oleg S. Pokrovsky<sup>2,3\*</sup>

6

7 <sup>1</sup> Institute of Ecological Problems of the North, N. Laverov Federal Center for Integrated Arctic  
8 Research, Nab Severnoi Dviny 23, Arkhangelsk 163000, Russia

9 <sup>2</sup> Geoscience and Environment Toulouse, UMR 5563 CNRS, University of Toulouse, 14 Avenue  
10 Edouard Belin, Toulouse 31400, France

11 <sup>3</sup> BIO-GEO-CLIM Laboratory, Tomsk State University, 35 Lenina Pr., Tomsk 634050, Russia

12

13 \*corresponding author email: [oleg.pokrovsky@get.omp.eu](mailto:oleg.pokrovsky@get.omp.eu)

14 Key words: bog, lake, stream, organic matter, metal, bacteria, sunlight

15

16 Synopsis:

17

18 In boreal (non-permafrost) humic (>15 mg DOC/L) waters of a stratified lake and an  
19 ombrotrophic bog, the experimentally measured rate of DOM photodegradation is 4 times higher  
20 than that of biodegradation. However, given the shallow (0.5 m) photic layer versus the full depth  
21 of water column (2 - 10 m), the biodegradation may provide the largest contribution to aerial  
22 CO<sub>2</sub> emission.

23

24

25

26

27

28

29

30

31

32



33 **Abstract**

34 Studying competitive effects of microbial and light-induced degradation of dissolved  
35 organic matter (DOM) is crucially important for understanding the factors controlling aquatic  
36 carbon (C) transformation in boreal waters. However, studies addressing both DOM and trace  
37 element (TE) behavior are limited, which does not allow assessment of coupled C – TE  
38 (including macro- and micronutrients and toxicants) biogeochemical cycles in these  
39 environmentally important settings. Here we conducted a seasonally-resolved assessment on the  
40 degree of DOM and related major and TE transformation under biotic activity and sunlight using  
41 conventional incubations of humic surface waters from the European subarctic. We studied bio-  
42 and photodegradation over 2 - 3 weeks in an ombrotrophic peatbog continuum (subsurface water  
43 from piezometer - small peatland pool - outlet stream) during July, and in three horizons (0.5, 5  
44 and 10 m) of deep (30 m), a stratified forest lake from the same region during June, August and  
45 September.

46 Along the bog water continuum in July, biodegradation rate was the highest in subsurface  
47 waters collected via piezometer and the lowest in the acidic peatland pool (0.17 to 0.03 mg C L<sup>-1</sup>  
48 d<sup>-1</sup>, respectively). Photodegradation was similar for piezometrically collected subsurface waters  
49 and the stream (about 0.3 mg C L<sup>-1</sup> d<sup>-1</sup>), but was not detectable in the peatland pool. The waters  
50 of forest lake exhibited a strong seasonal effect of biodegradation, which was the highest in  
51 October and the lowest in June (0.04 and 0.02 mg C L<sup>-1</sup> d<sup>-1</sup>, respectively). The photodegradation  
52 of DOM from the forest lake was observed only in June and August (0.19 and 0.07 mg C L<sup>-1</sup> d<sup>-1</sup>,  
53 respectively). Biodegradation was capable of removing between 1 and 7 % of initial DOC,  
54 being the highest in the forest lake in October and in peatland pool in summer. The photolysis  
55 was capable of degrading a much higher proportion of the initial DOC (10-25 %), especially in  
56 the forest lake during June and the bog stream during July. The change of optical parameters  
57 confirmed the highest photodegradation occurs in June (Arctic summer) and demonstrates a



58 decrease of chromophoric (aromatic) compounds during incubation, whereas biodegradation  
59 acted preferentially on aliphatic, low molecular weight compounds. Only a few trace metals were  
60 sizably affected by both photo- and biodegradation of DOM (Fe, Al, Ti, Nb and light REE),  
61 whereas V, Mn, Co, Cu and Ba were affected solely by biodegradation. Typical values of TE  
62 removal over a 2-week period of incubation ranged from 1 to 10 %. These effects were mostly  
63 pronounced in the less acidic forest lake compared to the bog waters. A likely mechanism of TE  
64 removal was their coprecipitation with coagulating Fe(III) hydroxides.

65 When averaged across sites and seasons, DOM biodegradation and photodegradation  
66 processes could remove 5.3 and 10.8 mg C L<sup>-1</sup> y<sup>-1</sup>, respectively. Compared to typical CO<sub>2</sub>  
67 emissions from inland waters of the region, biodegradation of DOM can provide the totality of  
68 C-CO<sub>2</sub> evasion from lake water surfaces whereas bio- and photodegradation are not sufficient to  
69 explain the observed fluxes in bog water continuum. Overall, these results demonstrated strong  
70 spatial and seasonal variability in DOM and TE complexes bio- and photodegradation, which  
71 was poorly accessed until now, and call for the need of a systematic assessment of both processes  
72 across seasons with high spatial resolution.

73

## 74 **1. Introduction**

75 Organic Carbon (OC) processing via metabolic biological (heterotrophic bacteria uptake  
76 and respiration) and inorganic physico-chemical (photolysis) pathways is considered to be one  
77 of the major source of CO<sub>2</sub> supersaturation in surface waters and related C emissions (Lapierre  
78 et al., 2013; Tranvik et al., 2009), although the relative role of dissolved vs particulate organic  
79 carbon (POC) remains poorly quantified (e.g. Attermeyer et al., 2018; Lau et al., 2021; Shirokova  
80 et al., 2021; Raudina et al., 2022). Given sizable C emissions in boreal and subarctic waters  
81 (Karlsson et al., 2021), together with high concentrations of DOC (Cole et al., 2007; Vonk et al.,  
82 2015), and fast ongoing and predicted environmental changes in high latitude aquatic and



83 terrestrial ecosystems (Wauthy et al., 2018; Chaudhary et al., 2020; Harris et al., 2022), the  
84 surface waters of subarctic regions are at the forefront of studies on the biogeochemical cycle of  
85 C. Although emissions from these waters are significantly lower than those in the 10 °S – 10 °N  
86 equatorial belt (e.g., Borges et al., 2015), the magnitude of possible changes in C flux from  
87 northern waters to the atmosphere remains much less known. Further, there are still important  
88 geographical biases linked to insufficient knowledge of rates and mechanisms of DOC  
89 transformation in certain regions. An example is peatland dominant northern aquatic settings,  
90 where high concentrations of soil organic C surrounding the bogs provide elevated  
91 concentrations of DOC. These soils and their organic C content become highly vulnerable to  
92 biological and physico-chemical impact depending on local environmental context, permafrost  
93 presence and season (Vonk et al., 2015).

94       Thorough laboratory and field work on DOM bio- and photolability conducted over the  
95 past decades have demonstrated both phenomena are important, and, depending on  
96 environmental setting (nutrient regime, photic layer depth, nature of DOM, etc.), one or another  
97 may dominate overall DOM removal in surface waters (Vachon et al., 2016, 2017; Vähätalo and  
98 Wetzel, 2008; Obernosterer and Benner, 2004). Recently, specific attention was devoted to the  
99 aquatic systems of permafrost peatlands given their high vulnerability to climate warming and  
100 huge potential for release of soil organic C to surfaces waters (Vonk et al., 2015; Shirokova et  
101 al., 2019; Payandi-Rolland et al., 2020; Prijac et al., 2022; Rosset et al., 2022; Taillardet et al.,  
102 2022). These former studies provided a range of DOM susceptibility to biotic degradation. Thus,  
103 between 10 and 40 % of the DOC in lakes, rivers and soil waters of the boreal zone may be  
104 available for bacterial uptake over a time frame of several weeks (Berggren et al., 2010; Roehm  
105 et al., 2009). This range is consistent with 14-16% of biodegradable DOC (BDOC) assessed  
106 globally (Begum et al. 2022). The necessity for further studies was also indicated, most notably  
107 with regard to *i*) seasonal aspects, given that the overwhelming majority of available studies were



108 performed during Arctic summer (see discussions in Vonk et al., 2015; Laurion et al., 2021), and  
109 *ii*) increased spatial resolution, given that sizable variations of BDOC can be observed within  
110 quite short distances of a hydrological continuum (Payandi-Rolland et al., 2020; Raudina et al.,  
111 2022). Another poorly studied aspect is DOM photo- and biolability across the depth of the water  
112 column, especially in seasonally stratified lakes which are subject to spring and autumn overturn.

113         Based on a compilation of available studies on BDOC and their own research, Vonk et  
114 al. (2015) argued there is a negligible amount of biodegradable DOC in aquatic systems without  
115 permafrost. This is, however, contradictory to available assessments on biodegradation of aquatic  
116 DOM as major driver of CO<sub>2</sub> emission in general (Amaral et al., 2021; Liu and Wang, 2022) and  
117 in boreal waters in particular (Ask et al., 2012; Lapierre et al., 2013). Furthermore, among all  
118 Arctic rivers, the highest annual (20%) and winter (ca. 45%) biodegradable DOC (BDOC) was  
119 reported for the Ob River, which drains through peatlands with minimal permafrost influence  
120 (Wickland et al., 2012). These non-exhaustive examples illustrate certain inconsistency in  
121 current estimations of DOC biodegradability in surface organic-rich waters of high latitudes,  
122 which precludes quantitative modeling of future C fluxes between land, water and atmosphere in  
123 these environmentally important regions. Towards addressing these inconsistencies, in this study,  
124 we chose a typical hydrological continuum in a boreal ombrotrophic bog in a glacial lake-ridge  
125 complex that includes subsurface water, a small peatland pool in the central part of the bog and  
126 an outlet stream. Further, we selected a well-studied deep stratified humic lake in the same region  
127 (Lake Temnoe; Chupakov et al., 2017) where we sampled surface and deep horizons for the  
128 incubation experiments. The chosen waters represent subarctic non-permafrost regions that  
129 exhibit sizable organic C pool in their soils and high concentrations of DOC in their surface  
130 waters. In contrast to previous studies of permafrost peatlands (Shirokova et al., 2019; Laurion  
131 et al., 2021; Payandi-Rolland et al., 2020; Mazoyer et al., 2022) where the main source of DOM  
132 is peat or ground vegetation like mosses and lichens, in this highly productive southern taiga



133 region, DOC may be more vulnerable to microbial activity due to the presence of forest leachates  
134 (i.e., Don and Kalbitz, 2005; Kalbitz et al., 2003; Kawahigashi et al., 2004; Kiikkilä et al., 2013)  
135 and much higher bioproductivity for both the terrestrial and aquatic parts of the lake-river  
136 ecosystems.

137         The working hypothesis behind our study design is that the DOC-rich subsurface water  
138 and deep horizons of the humic lake are mostly sensitive to sunlight impact (Stubbins et al.,  
139 2010), and that maximal impact of photodegradation is expected during allochthonous aromatic  
140 DOM input (high surface inflow to lakes and bogs in June and October). In contrast, maximal  
141 biodegradation of DOM is expected during periods of possible phytoplankton bloom in August,  
142 when autochthonous organic material is generated in the water column. Trace metals (TM) are  
143 supposed to either be taken up by biotic processing of DOM (e.g., micronutrients), or follow the  
144 transformation of colloidal organically-bound Fe/Al into particulate Fe, Al hydroxides (e.g.,  
145 Kopacek et al., 2005, 2006), capable of scavenging TM. To test these hypotheses, we examined  
146 DOM and related trace metals bio- and photodegradability aiming to assess 1) spatial variations  
147 along a hydrological continuum of non-permafrost peatland and different horizons of a  
148 neighboring deep stratified lake located in the forest, and 2) temporal variability during 3 main  
149 hydrological seasons (high flow in June, baseflow in August and autumn rain season in October)  
150 in the forest lake. Achieving these objectives should allow quantifying the relative share of bio-  
151 and photodegradation on overall DOC and TM removal from surface waters via biotic and  
152 physico-chemical mechanisms.

153

## 154 **2. Materials and Methods**

### 155 *2.1. Natural settings of subarctic bog and stratified lake*

156         The study site is in the NE part of the European boreal zone (Arkhangelsk region), **Fig.**  
157 **1.** The mean annual air temperature is 0 °C and average annual precipitation is 700 ± 50 mm.



158 The pristine ombrotrophic Ilasskoe Bog is located 30 km SE of Arkhangelsk, and is a typical  
159 lake-ridge complex formed from the last glaciation approximately 10,000 years ago. Its total  
160 surface area is 89 km<sup>2</sup>, with an average peat thickness of 3 m. The hydrological continuum of the  
161 Ilasskoe Bog includes subsurface water collected via piezometer (2-2.5 m depth), a small lake  
162 (Severnoe) and a stream outlet (**Fig. 1**). Lake Severnoe, located in the central part of the bog, is  
163 a typical peatland pool with an average depth of 1.5 m and a surface area of 0.013 km<sup>2</sup>. The  
164 Chernyi Stream is an outlet for the eastern part of the bog. The stream is 0.7-2.0 m wide, 10 km  
165 long and it flows in a forested (taiga) zone in the shade of tree canopy. The waters of the Ilasskoe  
166 Bog are acidic (pH ranges from 3.9-4.0 in piezometer and peatland pool to 5.7 in stream Chernyi),  
167 organic-rich (DOC is equal to 88, 13 and 38 mg L<sup>-1</sup> in the piezometer, lake and stream,  
168 accordingly) and lesser mineralized (Electrical Conductivity is 17-46 μS cm<sup>-1</sup>), as listed in **Table**  
169 **1**.

170 Lake Temnoe is located in a pristine forest 100 km NNE of the town of Arkhangelsk, an  
171 area that does not receive any direct anthropogenic impact (**Fig. 1**). The watershed area is 3.08  
172 km<sup>2</sup> and the lake surface area is 0.091 km<sup>2</sup>, with a maximum depth is 37 m and a Secchi disk  
173 depth of 3.5±0.5 m. The water residence time in the lake is 394 days. Bogs constitute 31% of  
174 lake's watershed area, which is represented by carbonate-free loamy moraine atop the peat,  
175 podzol and gley soils. The lake water is slightly acidic (pH = 5.1 to 6.0) and humic (DOC = 13-  
176 20 mg L<sup>-1</sup>) and dominated by allochthonous DOM with a low concentration of total dissolved  
177 ions (Electrical Conductivity of 20 μS cm<sup>-1</sup>). Similar to other deep boreal and subarctic lakes, the  
178 lake exhibits 2 main periods of pronounced stratification (November to April and June to  
179 September) and two periods of lake overturn (October and May). Maximal winter stratification  
180 occurs in March; the highest water temperature typically occurs in July (see Chupakov et al.,  
181 2017 for details).



182           The surface waters were collected from the shore (peatland pool and stream) or a PVC  
183 boat (Lake Temnoe). Surface (30-50 cm depth) waters were sampled in the Ilasskoe bog and 3  
184 water horizons (0.5, 5 and 10 m) were sampled in the Temnoe Lake using a pre-cleaned  
185 polycarbonate horizontal water sampler (Aquatic Research Co, ID, USA). The water samples  
186 were placed into 2-L Milli-Q pre-cleaned PVC jars and kept refrigerated until arrival at the  
187 laboratory within 2-3 hours of collection.

188

## 189           2.2. Experiments

### 190           2.2.1. Biodegradation

191           For biodegradation assessments we followed the recommended protocol and used the  
192 appropriate type of labware for assessing biodegradable DOC of Arctic waters without external  
193 nutrient addition (Vonk et al., 2015; Payandi-Rolland et al., 2020) and applied a slight  
194 modification from Shirokova et al. (2019) to assess maximal possible biodegradation. Initial  
195 water samples brought to the laboratory within 2-3 hours after sampling were filtered through 3  
196  $\mu\text{m}$  sterilized Nylon Sartorius membranes (47 mm diameter); these were used as ‘conventional’  
197 0.7  $\mu\text{m}$  (GF/F) filtration membranes might remove too many microbial cells (Dean et al., 2018).

198           Duplicate 30 mL aliquots of 3  $\mu\text{m}$ -filtered water were placed into pre-combusted (4.5  
199 hours at 450°C) dark borosilicate 40 mL glass bottles wrapped in Al foil to prevent any  
200 photolysis, without nutrient amendment and incubated at 22±1°C in the dark. The bottles were  
201 closed with loosened sterilized PVC caps. The bottles were shaken manually once a day avoiding  
202 the liquid touching the cap. The entire reactor was used for sampling after 0, 2, 5, 8, 12, and 21  
203 days of exposure. Sampled solutions were filtered through sterile, MilliQ-cleaned Sartorius 0.22  
204  $\mu\text{m}$  filters. The DOC blanks for these filters did not exceed 1% of DOC concentrations in  
205 experimental samples. Sterilized control reactors were filled with natural water that was filtered





206 through a 0.22  $\mu\text{m}$  sterile filter and incubated together with experimental reactors following the  
207 approach of Köhler et al (2002).

208 All handling and sampling of bottles was performed in the laminar hood box in a sterilized  
209 workspace. Filtered samples were acidified with 30  $\mu\text{L}$  of concentrated (8.1 M) double distilled  
210 HCl, tightly capped and stored in the refrigerator before DOC analyses. The non-acidified portion  
211 of filtrate was used for pH, Specific Conductivity, DIC and UV<sub>254 nm</sub> and optical spectra  
212 measurement. Control runs were 0.22  $\mu\text{m}$  sterile-filtered water which was incubated in parallel  
213 with experiments and re-filtered through 0.22  $\mu\text{m}$  filters the day of sampling. To ensure  
214 minimized release from sterilized Nylon membrane, we ran blank (Milli-Q) filtrations through  
215 both 0.7  $\mu\text{m}$  GF/F and 0.22  $\mu\text{m}$  Nylon filters; in both cases the DOC blank was below 0.1-0.2  
216 mg/L which is less than 1% of DOC concentration in our samples. The glass bottles were  
217 incubated in duplicates at  $22\pm 1^\circ\text{C}$  and agitated manually at least once a day over the 16 days of  
218 exposure.

219

### 220 2.2.2. Photodegradation

221 For photodegradation incubations, water samples were collected in Al-foil covered pre-  
222 cleaned polypropylene jars and sterile filtered (0.22  $\mu\text{m}$  Nalgene Rapid-Flow Sterile Systems)  
223 within 2 hours of sampling and refrigerated. The filtrates were transferred under laminar hood  
224 box into sterilized, acid-washed quartz tubes (150 mL volume, 20% air headspace) with silicate  
225 stoppers and placed at  $3 \pm 2$  cm depth into an outdoor pool which was filled by river water having  
226 the light transparency similar to that of the Ilasskoe and Temnoe lakes. In-situ measurements of  
227 sunlight intensity were conducted using a submersible sunlight sensor. The outdoor pools were  
228 placed in an unshaded area with a latitude similar to the sampling sites ( $< 30$  km from Ilasskoe  
229 Bog and Temnoe Lake). Slight wind movement and regular manual shaking allowed for  
230 sufficient mixing of reactor interiors during exposure. All photodegradation experiments were



231 run in duplicates. The water temperature (EBRO EBI 20) and light intensity (Luxmeter Testo  
232 545) were continuously recorded every 3 hours.

233 For photodegradation experiments, we followed conventional methods requiring  
234 exposure of 0.2  $\mu\text{m}$ -sterile filtered samples in quartz reactors in the outdoor pool (Vähätalo et al.,  
235 2003; Chupakova et al., 2018; Gareis and Lesack, 2018), solar simulator (Lou and Xie, 2006;  
236 Amado et al., 2014) or directly in the lake water (Laurion and Mladenov, 2013; Groeneveld et  
237 al., 2016). Note that the 0.22  $\mu\text{m}$  sterile filtration is the only way of conducting photodegradation  
238 experiments, given that autoclave sterilization of DOM-rich natural waters would coagulate  
239 humic material and thereby would not be suitable (Andersson et al., 2018). Filtration through a  
240 smaller pore size, however, would decrease the concentration of DOC and trace metals (i.e., Ilina  
241 et al., 2014; Vasyukova et al., 2010). We have chosen a 16 day exposure time for consistency  
242 with biodegradation experiments described above and following the previous studies on  
243 photodegradation under sunlight, which typically ranges from 15 to 70 days (Moran et al., 2000;  
244 Vähätalo and Wetzel, 2004; Mostofa et al., 2007; Chupakova et al., 2018). Dark control  
245 experiments were conducted also in duplicates, using sterilized glass tubes filled with sterile 0.22  
246  $\mu\text{m}$ -filtered water, wrapped in Al foil and placed in the same outdoor pool as the experiments.  
247 The headspace (approx. 20% of total reaction volume) was similar in experimental and control  
248 reactors. The individual reactors were sterile sampled at the beginning and after the 0, 2, 5, 8, 12,  
249 and 16 days of exposure. Each sampling sacrificed the entire reactor. The Milli-Q blanks were  
250 collected and processed to monitor for any potential sample contamination introduced by our  
251 filtration, incubation, handling and sampling procedures. The organic carbon blanks of the  
252 filtrates did not exceed 0.2 mg/L.

253

254

255



256           2.3. *Analyses*

257           The temperature, pH, O<sub>2</sub> and specific conductivity in surface waters were measured in  
258 field. The dissolved CO<sub>2</sub> concentration in the studied bodies of water was measured in-situ using  
259 submersible Vaissala Carbocap® GM70 handheld carbon dioxide meter with GMP222 probes  
260 (accuracy 1.5%; see Serikova et al. (2018, 2019) for methodological details). The diffusional  
261 CO<sub>2</sub> flux was calculated using a wind-based model (Cole and Caraco, 1998) with  $k_{600}$   
262  $= 2.07 + 0.215 \times u_{10}^{1.7}$ , where  $u_{10}$  is the wind speed at 10 m height, following the approaches  
263 developed for surface waters of peatlands (Zabelina et al., 2021).

264           The DOC and DIC were analyzed by high-temperature catalytic oxidation using a  
265 Shimadzu® TOC-VCSN (uncertainty  $\pm 2\%$ , 0.1 mg L<sup>-1</sup> detection limit). DIC was measured after  
266 sample acidification with HCl and DOC was analyzed in acidified samples after sparging it with  
267 C-free air for 3 min at 100 mL min<sup>-1</sup> as non-purgable organic carbon (NPOC). Internationally  
268 certified water samples (MISSISSIPPI-03 and Pérade-20) were used to check validity and  
269 reproducibility of the analysis. Filtered samples collected from photodegradation experiments  
270 were acidified with ultrapure nitric acid and analyzed for major and TE following the procedures  
271 employed by GET (Toulouse) for analyses of boreal humic waters (Oleinikova et al., 2017,  
272 2018).

273           The UV- and visual absorbance of water samples was measured using a 10 mm quartz  
274 cuvette on a CARY-50 UV-vis spectrophotometer to assess the aromaticity of pore fluids via  
275 specific UV absorbance (SUVA<sub>254</sub>). In the filtrates, we measured optical density at 254 nm and  
276 at select wavelengths (365, 436, 470, and 665 nm) as well as the entire UV-visible spectrum. The  
277 specific UV-absorbency (SUVA<sub>254</sub>, L mg<sup>-1</sup> m<sup>-1</sup>) and E<sub>470</sub>:E<sub>665</sub> ratios are used as a proxy for  
278 degree of condensation of aromatic groups of DOM, or humification (Chin et al., 1994; Weishaar  
279 et al., 2003; Hur et al., 2006; Peacock et al., 2013). The ratio E<sub>254</sub>:E<sub>436</sub> is useful for evaluation  
280 of contributions of autochthonous (aquatic) DOM compared to terrestrial (soil) C (Hur et al., 2006;



281 Ilina et al., 2014). The ratio  $E_{254}:E_{365}$  also allows approximating the mean molecular weight of  
282 DOM (Hiriart-Baer et al., 2008; Berggren et al., 2007). For better visualization of the differences  
283 in spectral parameters between experimental and control reactors, we calculated the difference  
284 ( $\Delta A$ ) between the absorbance of the photo- or bio-reactor and that of the control reactor at each  
285 sampling time.

286 Major cations, Si, P and ~40 TE were measured with a quadrupole ICP-MS (Agilent 7500  
287 ce) using In and Re as internal standards. The international geo-standard SLRS-5 (Riverine Water  
288 Reference Material for Trace Metals) was used to check validity and reproducibility of analyses.  
289 Note that for both bio- and photodegradation experiments, ICP MS analyses were performed  
290 over 16 days of incubation time.

291 To check for possible microbial development in biodegradation experiments, we  
292 performed oligotrophic and eutrophic bacteria counts over the course of incubation, following  
293 the standard methodology used in biodegradation experiments of peat waters (Stutter et al., 2013)  
294 and also described previously (Shirokova et al., 2017b; Chupakova et al., 2018).

295

#### 296 *2.4. Data treatment*

297 The bio- and photodegradable DOC and trace metals were calculated as percent loss  
298 relative to control in similar fashion with other studies (Vonk et al., 2015; Chupakova et al.,  
299 2018; Shirokova et al., 2017b, 2019). However, previous works in similar environmental contexts  
300 of high-DOC humic waters demonstrated that the effects of DOC and element decrease are rather  
301 low and often comparable to uncertainties of duplicates (Shirokova et al., 2019). To assess the  
302 net effect of bio- or photodestruction during the experiment, we used the integral values of  
303 concentration change, estimated as the difference between the experiment and the control, while  
304 taking into account the standard deviation of replicates. For this, we first calculated the mean of  
305 replicates at the  $i$ -th time of sampling for the experiment and the control of  $X$  component ( $^{mean}X_i$



306 and  $^{control}X_i$ , respectively). We next calculated the sum of mean concentration of replicates and  
307 its standard deviation ( $^{mean}X_i + SD_i$ ). Thus, we obtained 3 values characterizing the bio- or photo-  
308 degradation process: 1) the change of concentration in the experimental reactor ( $^{mean}S$ ), 2) the  
309 change of concentration not linked to the studied process ( $^{control}S$ ), and 3) the maximal uncertainty  
310 of the concentration change in the reactor ( $^{mean+SD}S$ ). This allowed calculating, in percentages,  
311 the efficiency of bio or photodegradation of  $X$  component relative to the control, taken into  
312 account relevant uncertainties as following:

$$313 \quad X (\%) = 100 \times (|^{mean}X| - |^{control}X|) / |^{control}X| \quad (1)$$

$$314 \quad SD (\%) = 100 \times (|^{mean+SD}X| - |^{mean}X|) / |^{control}X| \quad (2)$$

315 where  $X$  is biodegradable DOC or trace element (BDOC and BTE, respectively) or  
316 photodegradable DOC and trace element (PDOC and PTE, respectively). The sign of  $X$   
317 designates either a decrease («-») or an increase («+») of solute concentration during the  
318 experiment. We considered the decrease of concentration significant when  $X (\%) > SD (\%)$ . In  
319 other cases, the change was non-systematic over the course of experiment or non-measurable  
320 using the experimental technique employed in the present study.

321 The mean rate of bio- or photodegradation of  $X$  component ( $V_X$ ) was calculated based on  
322 the overall change ( $\Delta X$ , in %) between the initial ( $X_0$ ) and final value normalized to overall  
323 duration of the experiment  $t$  (22 and 16 days for bio- and photodegradation, respectively):

$$324 \quad V_X = ((\Delta X / X_0) / t \quad (3)$$

325 The SD for rates of component change were calculated in a similar way.

326 The spectral differences between experimental and control reactors were presented as  $X$ -  
327  $Y$ - $Z$  diagrams where  $X$  is elapsed time,  $Y$  is wavelength, and  $Z$  is  $\Delta A$ . The data were plotted in  
328 a Surfer software package using triangulation with a linear interpolation method. Statistical  
329 treatment included the least squares method and the Pearson correlation, as the data were  
330 normally distributed. The ANOVA method was used to test the differences in the average DOC



331 and metal concentration versus time in incubation experiments and in the controls and to assess  
332 the difference between the light experiments and the dark control for photodegradation  
333 experiments. All calculations were performed in STATISTICA ver. 10 (StatSoft Inc.,Tulsa) at  $p$   
334 = 0.05).

335

### 336 **3. Results**

#### 337 *3.1. Field measured C concentration and calculated CO<sub>2</sub> fluxes*

338 The DOC concentration ranged from 13 to 21 mg L<sup>-1</sup> in Lake Temnoe, depending on  
339 depth and season. The CO<sub>2</sub> concentrations and fluxes increased from June to October and varied  
340 from 99 to 220 μmol L<sup>-1</sup> and 32 to 71 mmol CO<sub>2</sub> m<sup>-2</sup> d<sup>-1</sup>, respectively (**Table 1**). In Ilasskoe Bog  
341 hydrological continuum, the DOC decreased from 88 mg L<sup>-1</sup> in the peat soil water to 38 mg L<sup>-1</sup>  
342 in the outlet stream. The DOC concentration was generally similar (within ± 5 %) between 3, 0.8  
343 (GFF), 0.45 and 0.22 μm pore size filtration of the initial sample, which is in agreement with  
344 former size fractionation measurements for Arctic and subarctic systems (Vasyukova et al., 2010;  
345 Pokrovsky et al., 2012, 2016, Shirokova et al., 2019). The waters of Ilasskoe Bog continuum  
346 exhibited CO<sub>2</sub> supersaturation with respect to atmosphere (from 55 to 3300 μmol L<sup>-1</sup>) and  
347 calculated CO<sub>2</sub> emission (diffusion) flux ranging from 22 mmol CO<sub>2</sub> m<sup>-2</sup> d<sup>-1</sup> in the peatland pool  
348 to 1600 mmol CO<sub>2</sub> m<sup>-2</sup> d<sup>-1</sup> in the piezometer (**Table 1**).

349

#### 350 *3.2. DOC concentration evolution in the experiments*

##### 351 3.2.1. Biodegradation

352 In the Temnoe Lake, the range of DOC concentration change during 2-3 week incubation  
353 in the experimental reactors did not exceed 2 mg/L and typically remained within +0.5 to -1.5  
354 mg/L, which is typically less than 10% of the initial DOC amount (**Fig. 2 and Fig. S1** of the  
355 Supplement). The biodegradable DOC was both season and depth dependent and ranged from 2



356 to 6 % (**Table 2**). The integral 2-week rates of biodegradation (**Table 3, Fig. 3 A**) demonstrated  
357 the highest values during autumn at depths of 0.5 m and 10 m and the lowest values during June  
358 at all depths. The final 0-10 m water column- and season-averaged biodegradation rate in Lake  
359 Temnoe ranged from 0.02 to 0.04 mg DOC L<sup>-1</sup> d<sup>-1</sup>. Integral rates of bio-degradation in the 0-10  
360 m layer of the lake demonstrated a general increase over the entire open-water period (May to  
361 October; **Fig. 4**).

362 For Ilasskoe Bog, in the hydrological continuum studied during July, the BDOC was  
363 highest in the peatland pool (4.9 ± 1.4 %) and lowest in the outlet stream (3.1 ± 2.4 %; **Fig. 2** and  
364 **Fig. S1**). The integral rate of DOC biodegradation followed the order ‘piezometer >> stream >  
365 lake’ and ranged from 0.03 to 0.17 mg C L<sup>-1</sup> d<sup>-1</sup> (**Table 3, Fig. 3 A**).

366

### 367 3.2.2. Photodegradation

368 Compared to biodegradation, photodegradation demonstrated much higher values of  
369 PDOC and rates of reaction as well as higher variability among seasons and sites. In Lake  
370 Temnoe, the PDOC was the highest in June and the lowest in October (**Fig. 2 B** and **Table 2**).  
371 The maximal range of concentration change during 2-week period achieved 6-8 mg L<sup>-1</sup> (**Fig. S2**)  
372 which was 10 to 20 % of the initial [DOC] values. The rates strongly decreased from May-June  
373 to the end of summer – autumn. The depth integrated (0 to 10 m) rate of DOM photodegradation  
374 in Lake Temnoe ranged from 0 in October to 0.2 mg C L<sup>-1</sup> d<sup>-1</sup> in June (**Table 3; Fig. 4 B**).

375 In the Ilasskoe Bog hydrological continuum during July, the photodegradation rate  
376 followed the order “outlet stream > piezometer >> peatland pool” (**Fig. 3 B**), where integral  
377 values of photodegradation equaled to 0.27±0.04, 0.33±0.07, and 0±0.05 mg C L<sup>-1</sup> d<sup>-1</sup>,  
378 respectively (**Table 3**).

379

380



381 *3.3. Optical parameters of DOM*

382 3.3.1 Biodegradation

383 In Lake Temnoe, the  $SUVA_{254}$  remained relatively constant (4.2 to 4.6 L mg C<sup>-1</sup> m<sup>-1</sup>)  
384 across seasons and depths (**Table 1 B**). Over the course of biodegradation, the  $SUVA_{254}$  did not  
385 change significantly (i.e., less than 0.2 units, which is comparable to the variability of duplicates;  
386 **Fig. S3**). The ratio  $E_{254}:E_{436}$ , which is an indicator of humification, increased with incubation  
387 time in Lake Temnoe waters; the magnitude of this increase followed the order “0.5 m > 5 m >  
388 10 m” (**Fig. S4**). The ratio  $E_{254}/E_{365}$  also increased over the course of biodegradation,  
389 corresponding to an increase of mean molecular weight of DOM (Hiriart-Baer et al., 2008;  
390 Berggren et al., 2007). The ratio  $E_{365}/E_{470}$  also demonstrated the strongest increase in surface  
391 horizons and virtually no change in the deepest horizon (**Fig. S4**). An increase in the ratio  
392  $E_{470}:E_{665}$  corresponds to a decrease in the degree of aromaticity (humification). An increase in  
393 the ratio  $E_{254}:E_{436}$  signifies a decrease in contribution of autochthonous (aquatic) DOM compared  
394 to terrestrial (soil) C, whereas an increase in the  $E_{254}:E_{365}$  ratio characterizes removal of low  
395 molecular weights compounds.

396 In Ilaskoe Bog samples, the highest  $SUVA$  was observed in the water of the piezometer  
397 and the lowest in the stream, but the evolution of this parameter in the course of biodegradation  
398 was rather weak (**Fig. S4**). The  $E_{254}:E_{365}$  and  $E_{254}:E_{436}$  ratios increased with incubation time in  
399 the piezometer and decreased with time in the stream (**Fig. S4**). The optical ratios ( $E_{254}:E_{436}$ ,  
400  $E_{365}:E_{470}$ ,  $E_{470}:E_{665}$ ) increased in the peatland pool, suggesting an increase in the molecular  
401 weight and an increase in the ratio of aromatic to aliphatic compounds.

402 Complete spectral differences between the experimental and control samples  
403 demonstrated rather weak ( $\Delta A \leq 0.04$ ) changes of spectral parameters, mostly detectable after  
404 10-12 days of incubation (**Fig. S5**). These results were generally consistent with the discrete  
405 spectral parameters presented above and demonstrated maximal effects in the piezometer and





406 bog outlet stream. In Lake Temnoe, the maximal impact of biodegradation on spectral parameters  
407 was observed in June, at 0.5 m depth.

408

### 409 3.3.2. Photodegradation

410 Similar to the DOC concentration, the optical parameters of DOM more strongly evolved  
411 over the course of photodegradation compared to the biodegradation experiments. In the Temnoe  
412 Lake, the strongest decrease in  $SUVA_{254}$  was observed in the waters of all horizons in June. This  
413 decrease was less strong in October (**Fig. S6**). The  $E_{254}:E_{365}$  ratio demonstrated a sizable increase,  
414 mostly pronounced in June, with the lowest but still measurable increase in October. The  
415  $E_{254}:E_{436}$  ratio strongly decreased with exposure time throughout all seasons (10 m depth) and  
416 only in June in the surface horizons (**Fig. S7**). An increase in the ratio  $E_{254}:E_{365}$  over the course  
417 of photodegradation corresponded to an increase in mean molecular weight of DOM, likely due  
418 to coagulation. The ratios  $E_{365}:E_{470}$  and  $E_{470}:E_{665}$  decreased in all experiments with the Temnoe  
419 Lake waters (**Fig. S7**), suggesting a decrease in the degree of humification (Battin, 1998) and a  
420 decrease in the ratio of aromatic to aliphatic moieties.

421 The  $SUVA$  in Ilasskoe Bog waters remained stable during photodegradation of stream  
422 waters and piezometer and strongly decreased in the peatland pool (**Fig. S6**). The  $E_{254}:E_{436}$  ratio  
423 strongly increased in the peatland pool and exhibited measurable decrease in stream waters and  
424 piezometer, whereas the  $E_{365}:E_{470}$  ratio systematically decreased in all photodegradation  
425 experiments with the Ilasskoe Bog continuum (**Fig. S7**). Finally, the  $E_{470}:E_{665}$  ratio exhibited  
426 sizable decrease, in the order 'stream >> pool  $\geq$  piezometer'. The total spectral differences  
427 between experimental and control reactors were mostly pronounced in stratified forest lake  
428 waters in June ( $\Delta A = -0.4$  to  $-0.4$ ) and in the bog continuum in July, where effects were strongest  
429 in the piezometer and outlet stream waters ( $\Delta A$  parameter as high as  $-0.4$  (**Fig. S8**)).

430



431 *3.4. Bacterial number evolution during biodegradation experiments*

432           The number of cultivable eutrophic bacteria (EB) sizably (ca., 2 orders of magnitude)  
433 increased during biodegradation of Lake Temnoe waters. However, this evolution was not  
434 systematic in the course of incubation; there was a pronounced decrease after 2 weeks of  
435 exposure in June and August and rather stable concentration in waters of all horizons sampled in  
436 October (**Fig. S9**). Such maxima in June and August might be linked to consumption of  
437 substrate/nutrient limitations on bacterial growth. In Ilasskoe Bog continuum, the number of  
438 eutrophic bacteria decreased by an order of magnitude in the peatland pool and piezometer while  
439 remaining constant in the stream. The number of oligotrophic bacteria (OB) increased in waters  
440 of all Lake Temnoe horizons by ca. 2 orders of magnitude in August and October and 1 order of  
441 magnitude in June. In contrast, the OB number did not change or slightly decreased during  
442 incubations of waters from Ilasskoe Bog continuum (**Fig. S9**).

443

444 *3.5. Trace element patterns*

445 3.5.1 TE in biodegradation experiments

446           During biodegradation experiments, a number of components [Group 1] demonstrated a  
447 statistically significant ( $X > SD$ , Eqn. 1) decrease in concentration across the incubation period  
448 (**Table 2**): Al, Ti, Fe, Co, Cu, Ba, Nb, light REE (LREE) and Pb (as illustrated for Fe in **Fig. 5**)  
449 as well as Mn, V, and La (**Figs. S10, S11 and S12**, respectively). The most significant effects  
450 were observed for Fe in the 0-5 m horizon of Lake Temnoe (9 to 18 % in June, 6 to 13.5 % in  
451 August and 8 to 9.5 % in October) and 14% in the peatland pool of Ilasskoe Bog. Overall, for  
452 most elements except Fe and Mn, this increase was less pronounced than that of DOC; maximal  
453 effects were achieved for Lake Temnoe in August and October (V, Mn, Co, Cu, Ni, Nb, Hf, Pb  
454 and Th) and in June (Al and Ti). These elements are typically linked to DOM and Fe and present  
455 in the form of organic- and organo-mineral colloids. Certain elements [Group 2] did not



456 appreciably change their concentration ( $< 2\%$  decrease): Li, B, Na, Mg, K, Ca, Si, Ge, As, Rb,  
457 Sr, Mo, Sb, Mo and Ba. These elements are not linked to colloids of Fe(III) hydroxide and organic  
458 matter. Finally, some elements [Group 3] exhibited unstable behavior without systematic change  
459 in concentration during the exposure ( $X < SD$ , Eqns. 1-2): Cr, Zn, Cu, Sr, Cd, (Y, Zr), Cs, Tl and  
460 U. These elements cannot be considered as significantly impacted by the biodegradation process  
461 in Lake Temnoe water.

462 In the Ilaskoe Bog hydrological continuum, the most significant changes during  
463 biodegradation were observed in the peatland pool and outlet stream. Elements strongly ( $> 5-10$   
464 %;  $X > S.D.$  in Eqn. 1) affected by biodegradation were V, Fe, Ni, Ga, Y, LREEs and Pb.

465

#### 466 3.5.2. TE in photodegradation experiments

467 The elements affected by photodegradation also formed three groups similar to those  
468 impacted by biodegradation. Aluminum, Fe, trivalent and tetravalent hydrolysates (Ti, Ga, Zr,  
469 Y, LREE and Th) and Nb of [Group 1] significantly ( $> 2\%$ ;  $p < 0.05$ ) decreased their  
470 concentration during photolysis as illustrated for Fe in **Fig. 6**, and for Ti and Zr in **Figs. S13** and  
471 **S14**, respectively. The decrease of Fe was mostly pronounced in Lake Temnoe water from 10 m  
472 depth, whereas that of Ti and Zr was detectable for all horizons and seasons except in October.  
473 For the Ilaskoe Bog continuum, there was no systematic change in Fe concentration, whereas  
474 concentrations of Ti and Zr systematically decreased over the course of sunlight exposure (**Figs.**  
475 **S13, S14**). Alkali (Li, Rb), alkaline-earth metals (Mg, Ca, Sr, Ba), Si and oxyanions (As, Mo,  
476 Sb) of [Group 2] were weakly ( $< 2\%$ ) affected by photolysis. Finally, the remaining trace  
477 elements of [Group 3] did not exhibit any systematic evolution of concentration during exposure  
478 to sunlight, or these changes were inferior to the uncertainties of replicates ( $X < S.D.$  in Eqn. 1).

479 We found that, unlike for DOC, the magnitude of trace element concentration decrease  
480 during photodegradation was generally lower than that of biodegradation experiments. Overall,



481 the strongest effects were observed for Ti (3 to 9% in Lake Temnoe; 20% in Ilasskoe Bog), Ga  
482 (6 to 14%), Zr (14-17% in Lake Temnoe), Nb (8 to 13%) and Th (8 to 19% in the Temnoe Lake  
483 and up to 50% in the Ilasskoe Bog). These effects were mostly pronounced in the Temnoe Lake  
484 in June and August and in peatland pool of the Ilasskoe Bog (July).

485

#### 486 **4. Discussion**

##### 487 *4.1. Comparison between biodegradation and photolysis*

488 The impact of season on the biodegradable DOC could be tested only for Lake Temnoe  
489 because it was sampled during the 3 main hydrological periods. The maximal biodegradation of  
490 the lake water was observed during autumn, when large amount of labile fresh soil OM and plant  
491 litter were delivered to the lake from the watershed via surface runoff. The water temperature  
492 seems to be of secondary importance for the intensity and rate of DOM biodegradation. It is  
493 worth noting that the seasonal pattern of BDOC in the humic lake quantified in this study (Fig.  
494 4 A) contrasted with previous works on biodegradation of large Arctic streams and rivers whose  
495 BDOC decreased as the Arctic summer progressed (Vonk et al., 2015). Presumably, the input of  
496 fresh material (plant litter at the end of summer-autumn from the forested watershed of Lake  
497 Temnoe) provided elevated biodegradation in the water column at the end of the open water  
498 season. Another reason could be due to lake overturn in October and exposure of deep partially  
499 autochthonous, and thus biodegradable, DOM to the surface biota. This biodegradable DOM  
500 originated from leaching of organic detritus accumulated during summer months along the  
501 bottom lake horizons (Chupakov et al., 2017). A supply of limiting nutrients (N and P) to the  
502 upper 0-10 m layer during lake overturn could also promote such biodegradation in October.

503 The highest biodegradation rates in the uppermost sections of the bog hydrological  
504 continuum (piezometer, **Fig. 3 A**) are consistent with recent findings on organic-rich waters of  
505 permafrost peatlands (Shirokova et al., 2019; Payandi-Rolland et al., 2020) and earlier results on



506 headwaters, small streams and soil leachates (Roehm et al., 2009; Ilina et al., 2014; Mann et al.,  
507 2014, 2015; Larouche et al., 2015; Spencer et al., 2015; Vonk et al., 2015; Moody et al., 2013;  
508 Pickard et al., 2017; Dean et al., 2019). This could be due to the very short water residence time  
509 and freshly leached DOM in these water objects (i.e., Mann et al., 2012; Abbott et al., 2014;  
510 Payandi-Rolland et al., 2020), given that bioavailable DOM components leached from plant litter  
511 are rapidly utilized (Textor et al., 2018). At the same time, overly low BDOC (2-8 %) values,  
512 regardless of depth and season in humic lake and across the hydrological continuum of the bog  
513 (**Fig. 2 A**), are supportive of previous results for permafrost peatlands from the neighboring  
514 region (Shirokova et al., 2019). A general path for DOM spectral properties modification over  
515 the course of biodegradation consisted of an increase in aromaticity of DOM due to preferential  
516 uptake of non-humic low molecular weight (LMW) compounds. However, this was not  
517 accompanied by an increase in SUVA (**Fig. S3**). Presumably, the proportion of these compounds  
518 in the overall DOC level was quite low and could not impact SUVA evolution. Globally, the  
519 evolution of optical ratios was consistent with bacterial consumption of aliphatic LMW  
520 compounds and an increase in the overall aromaticity of DOM.

521       Concerning the seasonal variation of photodegradation in the deep humic lake, maximal  
522 effects were observed in June. These maximal effects likely occurred due to fresh terrestrial  
523 organic matter (plant litter) leached from the watershed and then efficiently processed during  
524 Arctic summer. By July, the majority of DOM in lake surface layers was already degraded; this  
525 was observed for both the deep stratified Lake Temnoe and shallow peatland pool samples. In  
526 the end of summer, photodegradable DOM occurred solely in the deep horizon (10 m) of the  
527 lake. However, in October, even this deep horizon did not exhibit photodegradable DOM,  
528 presumably due to low insolation and unfavorable temperatures. It should be noted that labile  
529 phenolic, carbohydrates, N-containing bases and smaller molecular weight compounds are  
530 abundant in litter leachates produced during initial decay stages (Kiikkilä et al., 2011, 2012,



531 2013; Hensgens et al., 2021). By July, most of the biodegradable DOM was already removed,  
532 and in October, the effects were much lower. Therefore, photolabile DOM is delivered from the  
533 forested watershed to the lake essentially during surface flux, at high water flow. It is then quickly  
534 removed from the water column, which was especially seen in the 0.5 and 5 m horizons of Lake  
535 Temnoe. Although labile organic matter from litter fall was also delivered during autumn high  
536 flow, presumably, during this period, the conditions for photolysis (low temperature, short  
537 daytime period and insufficient light) were not as favorable as those in June or August.

538 Photodegradation of waters from the Ilasskoe Bog continuum demonstrated maximal  
539 rates in soil waters from the piezometer (**Fig. 3 B**). During photolysis of humic water, a decrease  
540 in optical ratios ( $E_{365}:E_{470}$ ;  $E_{470}:E_{665}$ ) clearly indicated preferential degradation of humic aromatic  
541 compounds. The strong effect of photodegradation on DOM optical properties in the 650-500  
542 nm region may be linked to decomposition of complex DOM into smaller molecules, whereas a  
543 decrease of absorbance in the 230-400 nm region (**Fig. S8**) indicates destruction of aromatic  
544 compounds, progressively increasing over insolation time. A recent study of DOM photolysis in  
545 humic-rich forested streams demonstrated that high aromatic material was photochemically  
546 converted into smaller non-fluorescent molecules (Wilske et al., 2020).

547 Results obtained on the more important role of photodegradation over biodegradation are  
548 generally consistent with earlier reports on the dominance of photolysis for DOM processing in  
549 Arctic waters within North America (Cory et al., 2014; Ward et al., 2017), the Canadian  
550 temperate zone (Winter et al., 2007; Porcal et al., 2013, 2014, 2015), and Swedish headwater  
551 catchments (Köhler et al., 2002). According to former results for Scandinavian surface waters,  
552 the main impact of DOM photolysis is reflected by a decrease in the proportion of aromatic  
553 (colored) DOC and a rather small ( $\leq 10\%$ ) change in bulk DOC concentration (Groeneveld et  
554 al., 2016; Koehler et al., 2014), Canada (Laurion and Mladenov, 2013; Gareis and Lesack, 2018)  
555 and NW Russia (Oleinikova et al., 2017; Chupakova et al., 2018).



556 As a further perspective of this work, one has to consider biodegradation of photolytically  
557 altered DOM given that photo-oxidation is known to transform molecular structures into more  
558 bioavailable forms (e.g., Cory and Kling, 2018; Sulzberger et al., 2019) thereby stimulating  
559 microbial growth under sunlight, as is known for other Arctic and subarctic settings (i.e.,  
560 Drozodova et al., 2020; Laurion et al., 2020).

561

562 *4.2. Possible impact of microbial and photolytic processing on CO<sub>2</sub> emissions from*  
563 *water surfaces*

564 The integral rates of DOM bioprocessing in the water column of Lake Temnoe (**Table 3**,  
565 **Fig. 4 A**) allow quantifying the potential contribution of biodegradation to CO<sub>2</sub> production and  
566 emission. Assuming all biodegraded DOM is transformed into CO<sub>2</sub> and there is no biomass  
567 increase or sedimentation, a 1 m water layer of the lake can emit 0.02 g C-CO<sub>2</sub> m<sup>-2</sup> d<sup>-1</sup> in June  
568 and 0.04 g C-CO<sub>2</sub> m<sup>-2</sup> d<sup>-1</sup> in October. Assuming the entire water column studied in this work (10  
569 m depth of Lake Temnoe) participates in DOM biodegradation and CO<sub>2</sub> emission, the integral  
570 flux amounts to 0.2-0.4 g C-CO<sub>2</sub> m<sup>-2</sup> d<sup>-1</sup> across the seasons. These values are comparable to  
571 typical values of CO<sub>2</sub> evasion from the surface of this lake during different seasons (30-70 mmol  
572 CO<sub>2</sub> m<sup>-2</sup> d<sup>-1</sup>, or 0.36-0.84 g C-CO<sub>2</sub> m<sup>-2</sup> d<sup>-1</sup>; **Table 1 B**).

573 For surface waters of Ilasskoe Bog, maximal CO<sub>2</sub> production due to DOM  
574 biomineralization alone (**Table 3**) ranged from 0.06 g C-CO<sub>2</sub> m<sup>-2</sup> d<sup>-1</sup> for the peatland pool (2 m  
575 deep) to 0.03 g C-CO<sub>2</sub> m<sup>-2</sup> d<sup>-1</sup> for the outlet stream (0.5 m deep). However, in summer, the  
576 peatland pool and stream emitted 0.27 and 1.8 g C-CO<sub>2</sub> m<sup>-2</sup> d<sup>-1</sup> (**Table 1 A**) which could not be  
577 sustained by DOM biodegradation.

578 The addition of photodegradation (assuming a photic layer depth of 3.5 m) to DOM  
579 bioprocessing in the water column of the Temnoe Lake during open water season can further  
580 increase potential CO<sub>2</sub> production in the water column thus making it possible to provide entire



581 observed CO<sub>2</sub> evasions. For the case of Ilasskoe Bog waters, the addition of photolytic  
582 degradation increases projected CO<sub>2</sub> emission from the outlet stream by a factor of 5, which is  
583 still below the actual CO<sub>2</sub> flux, whereas DOM photolysis has no impact on CO<sub>2</sub> emissions from  
584 the peatland pool. Note that, although the depth of sunlight processing in boreal waters is  
585 typically 1-0.8 m (Vähätalo et al., 2000; Koehler et al., 2014), a more recent study concluded that  
586 direct photomineralization of DOM in Arctic humic ponds is limited to the first centimeters of the  
587 water column (Mazoyer et al., 2022). Furthermore, in typical DOM-rich Arctic waters, only half  
588 of sunlight-associated DOC losses is converted into CO<sub>2</sub> and the rest may be turned into particles  
589 through photoflocculation (e.g., Mazoyer et al., 2022). Therefore, despite a faster  
590 photodegradation rate compared to biodegradation, due to the shallow photic layer in humic  
591 waters, the biodegradation may provide the largest impact on CO<sub>2</sub> emission from the water  
592 column of boreal waters.

593

#### 594 *4.3. Impact of DOM bio- and photo transformation on trace element cycling*

595 Among all major and trace elements measured in the experiments, only a few (trivalent  
596 and tetravalent hydrolysates, TE<sup>3+</sup>, TE<sup>4+</sup>) were impacted by both photo- and biodegradation. It is  
597 known that these elements are essentially present in the form of large molecular size, highly  
598 polymerized and presumably aromatic, organo-Fe/Al colloids in humic boreal/subarctic lakes  
599 (Pokrovsky et al., 2012, 2016), rivers (Krickov et al., 2019; Pokrovsky et al., 2010), and soil  
600 porewaters (Pokrovsky et al., 2005; Raudina et al., 2021). Therefore, insoluble TE<sup>3+</sup> and TE<sup>4+</sup>  
601 generally followed the removal of Fe(III) in the form of particulate Fe hydroxides, after breaking  
602 the Fe-DOM bonds that stabilized colloidal Fe(III) hydroxides. This destabilization and Fe  
603 hydroxide particle formation is known to occur either via biodegradation (i.e., Oleinikova et al.,  
604 2018) or photolysis (Kopacek et al., 2005, 2006; Oleinikova et al., 2017; Chupakova et al., 2018).  
605 At the same time, some micronutrients (V, Mn, Co, Cu and Ba) were affected solely by





606 biodegradation. This can reflect uptake of these metals by growing bacterial cells, as is known  
607 from laboratory experiments with pure cultures of heterotrophic bacteria (Shirokova et al.,  
608 2017a).

609 Note that the effects of bio- and photodegradation were more pronounced for light REE  
610 (LREE) compared to heavy REE (HREE). This result is consistent with the fact that LREE have  
611 stronger association with Fe hydroxide compared to organic complexes, as known from general  
612 chemical considerations and laboratory experiments (i.e., Bau, 1999) and evidenced in various  
613 boreal and subarctic settings (Pokrovsky et al., 2016; Krickov et al., 2019). Given that the main  
614 effect of both photolysis and biodegradation of DOM in humic Fe(III)-rich surface waters is  
615 coagulation of dissolved Fe(III) in the form of Fe oxy(hydr)oxides, the LREE are removed from  
616 solution [either in the form of adsorbed complexes or coprecipitated with Fe oxy(hydr)oxides]  
617 while HREE remain [in the form of strong aqueous complexes].

618 In former studies of photo- and biodegradation of surface waters from permafrost  
619 peatlands, only a few nutrients (P, Fe, Zn and V) and insoluble low mobility trace metals (Ti, Zr,  
620 Nb and Th) demonstrated a decrease in concentration (Shirokova et al., 2019). This list of  
621 elements is generally consistent with that established in the present study of humic subarctic  
622 lakes of the non-permafrost zone, except P and Zn which did not exhibit sizable removal in our  
623 experiments. It is possible that a high proportion of low molecular weight  $LMW_{< 1 \text{ kDa}}$  (and thus,  
624 potentially bioavailable) forms of macro- and micronutrients, such as P and Zn, in the permafrost  
625 ice (i.e., Kuzmina et al., 2023) can be delivered to the lake and river via suprapermafrost flow  
626 (Raudina et al., 2018, 2021), which is eventually responsible for elevated bioavailability of these  
627 elements in permafrost surface waters, as reported in former experiments.

628

629 **Conclusions**



630           Seasonally resolved bio- and photo-degradability of DOM in a deep stratified lake and  
631 summer measurements from a peat bog's hydrological continuum within the boreal zone  
632 confirmed the initial hypothesis that the subsurface and deep horizons of these stratified waters  
633 are mostly sensitive to sunlight impact, and that maximal effects of photodegradation occurred  
634 in the month of June during strong insolation. In contrast, the biodegradation of DOM from the  
635 humic lake was mostly pronounced during October, when fresh leachates of forest litter were  
636 exported from the watershed. The evolution of optical parameters of DOM demonstrated removal  
637 of aliphatic, presumably autochthonous, organic ligands during biodegradation and photolysis of  
638 aromatic humic molecules. Insoluble low-mobility trace metals such as trivalent and tetravalent  
639 hydrolysates were affected by both bio- and photodegradation, as they are associated with  
640 coagulating Fe(III) oxyhydroxides. A few micronutrients (V, Mn, Co, Cu and Ba) were, however,  
641 removed during biodegradation experiments, thus reflecting their possible uptake by  
642 microorganisms.

643           Although DOM photodegradation rates were sizably higher compared to those of  
644 biodegradation, the rather thin photic layer in humic waters does not allow for significant  
645 contribution of photolysis in overall CO<sub>2</sub> emission from lake and bog surfaces. In the deep  
646 stratified lake, the biodegradation alone was capable explaining observed CO<sub>2</sub> emissions, while  
647 in the shallow bog continuum, the sum of bio- and photodegradation were not sufficient to  
648 provide CO<sub>2</sub> flux. The high seasonal dynamics and spatial variability in both photo- and  
649 biodegradability of DOM and related trace elements of humic surface waters in the boreal zone  
650 encountered in this study suggest the need for further assessment of rates of these processes with  
651 focus on early spring and late autumn, the periods of maximal photo- and biodegradation,  
652 respectively. Considering the strong spatial variations of DOM processing in the aquatic  
653 continuum, focus should be centered on the most dynamic components such as small streams and  
654 subsurface waters, which demonstrated the highest rates of both photo- and biodegradation.



655

656 **Acknowledgements**

657 This work was supported by RSF grant No 22-17-00253. LS and OP were also supported  
658 by project PEACE of PEPR FairCarboN ANR-22-PEXF-0011. OP is grateful for partial support  
659 from the TSU Development Programme Priority-2030.

660

661 **Assets:** All the data obtained in this work are presented in Supplementary Information file.

662

663 **Authors contribution.**

664 AVC and OP designed the study and wrote the paper; AC and SB performed sampling, analysis  
665 and their interpretation; LS performed bacterial number assessment and DOC results  
666 interpretation; AVC and OP provided analyses of literature data

667

668 **Competing interests.**

669 The authors declare that they have no conflict of interest.

670

671 **References**

- 672 Abbott, B. W., Larouche, J. R., Jones, J. B., Bowden, W. B., and Balser, A. W.: Elevated  
673 dissolved organic carbon biodegradability from thawing and collapsing permafrost, *J.*  
674 *Geophys. Res.*, 119, 2049–2063, 2014.
- 675 Amado, A. M., Cotner, J. B., Cory, R. M., Edlund, B. L., and McNeill, K.: Disentangling the  
676 interactions between photochemical and bacterial degradation of dissolved organic matter:  
677 amino acids play a central role, *Microb. Ecol.*, 69(3), 554–566, 2014.
- 678 Amaral, V., Ortega, T., Romera-Castillo, C., and Forja, J.: Linkages between greenhouse gases  
679 (CO<sub>2</sub>, CH<sub>4</sub>, and N<sub>2</sub>O) and dissolved organic matter composition in a shallow estuary, *Sci.*  
680 *Total Environ.* 788, Art No 147863, 2021.
- 681 Andersson, M. G. I., Catalán, N., Rahman, Z., Tranvik, L. J., and Lindström, E. S.: Effects of  
682 sterilization on dissolved organic carbon (DOC) composition and bacterial utilization of  
683 DOC from lakes, *Aquat. Microb. Ecol.*, 82, 199–208, 2018.
- 684 Ask, J., Karlsson, J., and Jansson, M.: Net ecosystem production in clear-water and brown-water  
685 lakes, *Glob. Biogeochem. Cycles*, 26, GB1017, doi:10.1029/2010GB003951, 2012.
- 686 Attermeyer, K., Catalán, N., Einarsdóttir, K., Freixa, A., Groeneveld, M., Hawkes, J. A., et al.:  
687 Organic carbon processing during transport through boreal inland waters: Particles as  
688 important sites, *J. Geophys. Res.: Biogeosciences*, 123(8), 2412–2428.  
689 <https://doi.org/10.1029/2018jg004500>, 2018.
- 690 Bau, M.: Scavenging of dissolved yttrium and rare earths by precipitating iron oxyhydroxide:  
691 experimental evidence for Ce oxidation, Y-Ho fractionation, and lanthanide tetrad effect,  
692 *Geochim. Cosmochim. Ac.*, 63, 67–77, 1999.
- 693 Battin T.J. Dissolved organic materials and its optical properties in a blackwater tributary of the  
694 upper Orinoco River, Venezuela, *Organic Geochemistry*, 28, 561–569, 1998.



- 695 Begum, M. S., Park, J.-H., Yang, L., Shin, K. H., and Hur, J.: Optical and molecular indices of  
696 dissolved organic matter for estimating biodegradability and resulting carbon dioxide  
697 production in inland waters: A review. *Water Research*, Art No 119362, 2022.
- 698 Berggren, M., Laudon, H., and Jansson, M.: Landscape regulation of bacterial growth efficiency  
699 in boreal freshwaters, *Global Biogeochem. Cy.*, 21, GB4002.  
700 <http://dx.doi.org/10.1029/2006GB002844>, 2007.
- 701 Berggren, M., Laudon, H., Haei, M., Ström, L., and Jansson, M.: Efficient aquatic bacterial  
702 metabolism of dissolved low-molecular-weight compounds from terrestrial sources, *ISME*  
703 *J.*, 4, 408-416, 2010.
- 704 Borges, A., Darchambeau, F., Teodoru, C. et al. : Globally significant greenhouse-gas emissions  
705 from African inland waters, *Nature Geosci.*, 8, 637–642. <https://doi.org/10.1038/ngeo2486>,  
706 2015.
- 707 Chaudhary, N., Westermann, S., Lamba, S., et al.: Modelling past and future peatland  
708 carbon dynamics across the pan- Arctic, *Glob. Change Biol.*, 26, 4119-4133, 2020.
- 709 Chin, Y.-P., Aiken, G., and O’Loughlin, E.: Molecular weight, polydispersity, and spectroscopic  
710 properties of aquatic humic substances, *Environ. Sci. Technol.*, 28, 1853-1858, 1994.
- 711 Chupakov, A., Ershova, A., Moreva, O. Yu, Shirokova, L. S., Zabelina, S. A., Vorobieva, T.Ya.,  
712 Klimov, S. I., Brovkon N., Pokrovsky, O.S.: Seasonal dynamics of dissolved carbon in  
713 contrasting stratified lakes of the subarctic, *Boreal Environ. Res.*, 22, 213–230, 2017.
- 714 Chupakova, A. A., Chupakov, A. V., Neverova, N. V., Shirokova, L. S., and Pokrovsky, O. S.:  
715 Photodegradation of river dissolved organic matter and trace metals in the largest European  
716 Arctic estuary, *Sci. Total Environ.*, 622–623, 1343–1352, 2018.
- 717 Cole, J. J. and Caraco, N.: Atmospheric exchange of carbon dioxide in a low-wind oligotrophic  
718 lake measured by the addition of SF<sub>6</sub>, *Limnol. Oceanogr.*, 43, 647–656, 1998.
- 719 Cole, J. J., Prairie, Y. T., Caraco, N. F., McDowell, W. H., Tranvik, L. J., Striegl, R. G., Duarte,  
720 C. M., Kortelainen, P., Downing, J. A., Middelburg, J. J., and Melack, J.: Plumbing the  
721 global carbon cycle: Integrating inland waters into the terrestrial carbon budget, *Ecosystems*,  
722 10, 172–185, <https://doi.org/10.1007/s10021-006-9013-8>, 2007.
- 723 Cory, R. M., Ward, C. P., Crump, B. C., and Kling, G. W.: Sunlight controls water column  
724 processing of carbon in arctic fresh waters, *Science*, 345, 925-928, 2014.
- 725 Cory, R. M., and Kling, G. W.: Interactions between sunlight and microorganisms influence  
726 dissolved organic matter degradation along the aquatic continuum, *Limnol. Oceanogr. Lett.*,  
727 3, 102–116, 2018.
- 728 Dean, J. F., van Hal, J. R., Dolman, A. J., Aerts, R., and Weedon, J. T.: Filtration artefacts in  
729 bacterial community composition can affect the outcome of dissolved organic matter  
730 biolability assays, *Biogeosciences*, 15, 7141-7154, [https://doi.org/10.5194/bg-15-7141-](https://doi.org/10.5194/bg-15-7141-2018)  
731 2018, 2018.
- 732 Dean, J. F., Garnett, M. H., Spyrakos, E., Billett, M. F.: The potential hidden age of dissolved  
733 organic carbon exported by peatland streams, *J. Geophys. Res.: Biogeosciences*,  
734 124, 328–341, 2019.
- 735 Don, A., and Kalbitz, K.: Amount and degradability of dissolved organic carbon from foliar litter  
736 at different decomposition stages, *Soil Biol. Biochem.*, 37, 2171-2179, 2005.
- 737 Drozdova, O. Y., Aleshina, A. R., Tikhonov, V. V., Lapitskiy, S. A., and Pokrovsky, O. S.:  
738 Coagulation of organo-mineral colloids and formation of bioavailable low molecular weight  
739 organic complexes in boreal humic river water under UV-irradiation, *Chemosphere*, 250,  
740 Art No 126216, [doi.org/10.1016/j.chemosphere.2020.126216](https://doi.org/10.1016/j.chemosphere.2020.126216), 2020.
- 741 Gareis, J. A. L., and Lesack, L. F. W.: Photodegraded dissolved organic matter from peak  
742 freshet river discharge as a substrate for bacterial production in a lake-rich great Arctic delta,  
743 *Arctic Science*, 4(4), 557-583, 2018.



- 744 Groeneveld, M., Tranvik, L., Natchimuthu, S., and Koehler, B.: Photochemical mineralisation in  
745 a boreal brown water lake: considerable temporal variability and minor contribution to  
746 carbon dioxide production, *Biogeoscience*, 13, 3931–3943, 2016.
- 747 Harris, L. I., Richardson, K., Bona, K. A., Davidson, S. J., Finkelstein, S. A., Garneau, M.,  
748 McLaughlin, J., Nwaishi, F., Olefeldt, D., Packalen, M., Roulet, N. T., Southee, F. M.,  
749 Strack, M., Webster, K. L., Wilkinson, S. L., and Ray, J. C.: The essential carbon service  
750 provided by northern peatlands, *Front. Ecol. Environ.*, 20, 222–230,  
751 <https://doi.org/10.1002/fee.2437>, 2022.
- 752 Hengsgens, G., Lechtenfeld, O. J., Guillemette, F., Laudon, H., Berggren, M.: Impacts of litter  
753 decay on organic leachate composition and reactivity, *Biogeochemistry* 154, 99–117, 2021.
- 754 Hiriart-Baer, V.P., Diep, N., and Smith, R.E.H.: Dissolved organic matter in the Great Lakes: role  
755 and nature of allochthonous material, *J. Great Lakes Res.* 34, 383–394, 2008.
- 756 Hur, J., Williams, M. A., and Schlautman, M. A.: Evaluating spectroscopic and chromatographic  
757 techniques to resolve dissolved organic matter via end member mixing analysis, *Chemosphere*,  
758 63, 387–402, 2006.
- 759 Ilina, S. M., Drozdova, O. Yu., Lapitsky, S. A., Alekhin, Yu. V., Demin, V. V., Zavgorodnaya, Yu.  
760 A., Shirokova, L. S., Viers, J., and Pokrovsky, O. S.: Size fractionation and optical properties  
761 of dissolved organic matter in the continuum soil solution-bog-river and terminal lake of a  
762 boreal watershed, *Org. Geochem.*, 66, 14–24, 2014.
- 763 Kalbitz, K., Schmerwitz, J., Schwesig, D., and Matzner, E.: Biodegradation of soil-derived  
764 dissolved organic matter as related to its properties, *Geoderma* 113, 273–291, 2003.
- 765 Karlsson, J., Serikova, S., Rocher-Ros, G., Denfeld, B., Vorobyev, S. N., Pokrovsky, O. S.:  
766 Carbon emission from Western Siberian inland waters, *Nature Comm.*, 12, 825,  
767 <https://doi.org/10.1038/s41467-021-21054-1>, 2021.
- 768 Kawahigashi, M., Kaiser, L., Kalbitz, K., Rodionov, A., and Guggenberger, G.: Dissolved  
769 organic matter in small streams along a gradient from discontinuous to continuous  
770 permafrost. *Global Change Biol.* 10, 1576–1586, 2004.
- 771 Kiikkilä, O., Kitunen, V., and Smolander, A.: Properties of dissolved organic matter derived  
772 from silver birch and Norway spruce stands: Degradability combined with chemical  
773 characteristics, *Soil Biol. Biochem.* 43, 421–430, 2011.
- 774 Kiikkilä, O., Kitunen, V., Spetz, P., and Smolander, A.: Characterization of dissolved organic  
775 matter in decomposing Norway spruce and silver birch litter, *European J Soil Sci* 63, 476–  
776 486, 2012.
- 777 Kiikkilä, O., Smolander, A., and Kitunen, V.: Degradability, molecular weight and adsorption  
778 properties of dissolved organic carbon and nitrogen leached from different types of  
779 decomposing litter, *Plant Soil* 373, 787–798, 2013.
- 780 Koehler, B., Landelius, T., Weyhenmeyer, G. A., Machida, N., and Tranvik, L.J.: Sunlight-  
781 induced carbon dioxide emissions from inland waters, *Global Biogeochem. Cycles*, 28, 696–  
782 711, 2014.
- 783 Köhler, S., Buffam, I., Jonsson, A., and Bishop, K.: Photochemical and microbial processing of  
784 stream and soil water dissolved organic matter in a boreal forested catchment in northern  
785 Sweden, *Aquat. Sci.*, 64, 269–281, 2002.
- 786 Kopáček, J., Klementova, S., and Norton S. A.: Photochemical production of ionic and  
787 particulate aluminum and iron in lakes, *Environ. Sci. Technol.*, 39, 3656–3662, 2005.
- 788 Kopáček, J., Marešová, M., Norton, S. A., Porcal, P., and Veselý, J.: Photochemical source of  
789 metals for sediments, *Environ. Sci. Technol.*, 40(14), 4455–4459.  
790 <https://doi.org/10.1021/es0600532>, 2006.



- 791 Krickov, I. V., Pokrovsky, O. S., Manasypov, R. M., Lim, A., Shirokova, L. S., and Loiko, S.  
792 V.: Colloidal transport of carbon and metals by western Siberian rivers during different  
793 seasons across a permafrost gradient, *Geochim. Cosmochim. Acta* 265, 221-241,  
794 <https://doi.org/10.1016/j.gca.2019.08.041>, 2019.
- 795 Kuzmina, D., Lim, A. G., Loiko, S. V., Shirokova, L. S., Julien, F., Rols, J. L., and Pokrovsky,  
796 O. S.: Dispersed ice of permafrost peatlands represents an important source of labile  
797 carboxylic acids, nutrients and metals, *Geoderma*, 429, Art No 116256.  
798 <https://doi.org/10.1016/j.geoderma.2022.116256>, 2023.
- 799 Lapierre, J.-F., Guillemette, F., Berggren, M., and del Giorgio, P. A.: Increases in terrestrially  
800 derived carbon stimulate organic carbon processing and CO<sub>2</sub> emissions in boreal aquatic  
801 ecosystems, *Nature Comm.*, 4, 2972, doi:10.1038/ncomms3972, 2013.
- 802 Larouche, J. R., Abbott, B. W., Bowden, W. B., Jones, and J. B.: The role of watershed  
803 characteristics, permafrost thaw, and wildfire on dissolved organic carbon biodegradability  
804 and water chemistry in Arctic headwater streams, *Biogeosciences*, 12, 4221-4233, 2015.
- 805 Lau, M. P.: Linking the dissolved and particulate domain of organic carbon in inland waters. *J.*  
806 *Geophys. Res.: Biogeosciences*, 126, e2021JG006266.  
807 <https://doi.org/10.1029/2021JG006266>, 2021.
- 808 Laurion, I., and Mladenov, N.: Dissolved organic matter photolysis in Canadian Arctic thaw  
809 ponds, *Environ. Res. Lett.*, 8, 035026, doi.org/10.1088/1748-9326/8/3/035026, 2013.
- 810 Laurion, I., Massicotte, P., Mazoyer, F., Negandhi, K., and Mladenov, N.: Weak mineralization  
811 despite strong processing of dissolved organic matter in Eastern Arctic tundra ponds,  
812 *Limnol. Oceanogr.*, 66, S47–S63, <https://doi.org/10.1002/lno.11634>, 2021.
- 813 Liu, F., and Wang, D.: Dissolved organic carbon concentration and biodegradability across the  
814 global rivers: A meta-analysis, *Sci. Total Environ.*, 818, Art No 151828, 2022.
- 815 Lou, T., and Xie, H.: Photochemical alteration of the molecular weight of dissolved organic  
816 matter, *Chemosphere*, 65, 2333-2342, 2006.
- 817 Mann, P. J., Davydova, A., Zimov, N., Spencer, R. G. M., Davydov, S., Bulygina, E., Zimov, S.,  
818 Holmes, R. M.: Controls on the composition and lability of dissolved organic matter in  
819 Siberia's Kolyma River basin, *J. Geophys. Res.*, 117, G01028, doi: 10.1029/2011JG001798,  
820 2012.
- 821 Mann, P. J., Sobczak, W. V., LaRue, M. M., Bulygina, E., Davydova, A., Vonk, J. E., Schade,  
822 J., Davydov, S., Zimov, N., Holmes, R. M., Spencer, R. G. M.: Evidence for key enzymatic  
823 controls on metabolism of Arctic river organic matter, *Global Change Biol.*, 20(4), 1089-  
824 1100, 2014.
- 825 Mann, P. J., Eglinton, T. I., McIntyre, C. P., Zimov, N., Davydova, A., Vonk, J. E., Holmes, R.  
826 M., Spencer, R. G. M.: Utilization of ancient permafrost carbon in headwaters of Arctic  
827 fluvial networks, *Nat. Commun.*, 6, doi: 10.1038/ncomms8856, 2015.
- 828 Mazoyer, F., Laurion, I., and Rautio, M.: The dominant role of sunlight in degrading winter  
829 dissolved organic matter from a thermokarst lake in a subarctic peatland, *Biogeosciences*,  
830 19, 3959–3977, <https://doi.org/10.5194/bg-19-3959-2022>, 2022.
- 831 Moody, C. S., Worrall, F., Evans, C. D., Jones, T. G.: The rate of loss of dissolved organic carbon  
832 (DOC) through a catchment, *J. Hydrol.*, 492, 139-150, 2013.
- 833 Moran, M. A., Sheldon, W. M., and Zepp, R. G.: Carbon loss and optical property changes during  
834 long-term photochemical and biological degradation of estuarine dissolved organic matter,  
835 *Limnol. Oceanogr.*, 45, 1254–1264, 2000.
- 836 Mostofa, K. M. G., Yoshioka, T., Konohira, E., and Tanoue, E.: Photodegradation of fluorescent  
837 dissolved organic matter in river waters, *Geochem. J.*, 41, 323-331, 2007.



- 838 Obernosterer, I., and Benner, R.: Competition between biological and photochemical processes  
839 in the mineralization of dissolved organic carbon, *Limnol. Oceanogr.*, 49, 117–124,  
840 <https://doi.org/10.4319/lo.2004.49.1.0117>, 2004.
- 841 Oleinikova, O., Drozdova, O. Y., Lapitskiy, S. A., Bychkov, A. Y., and Pokrovsky, O. S.:  
842 Dissolved organic matter degradation by sunlight coagulates organo-mineral colloids and  
843 produces low-molecular weight fraction of metals in boreal humic waters, *Geochim.  
844 Cosmochim. Acta*, 211, 97–114, 2017.
- 845 Oleinikova, O., Shirokova, L. S., Drozdova, O. Y., Lapitskiy, S. A., and Pokrovsky, O. S.: Low  
846 biodegradability of dissolved organic matter and trace metal from subarctic waters by culturable  
847 heterotrophic bacteria, *Sci. Total Environ.*, 618, 174–187, 2018.
- 848 Payandi-Rolland, D.; Shirokova, L.S.; Tesfa, M.; Lim, A.G.; Kuzmina, D.; Benezeth, P.;  
849 Karlsson, J.; Giesler, R.; Pokrovsky, O.S.: Dissolved organic matter biodegradation along a  
850 hydrological continuum in a discontinuous permafrost area: Case study of northern Siberia  
851 and Sweden, *Sci. Total Environ.*, 749, Art No 141463, 2020.
- 852 Peacock, M., Evans, C. D., Fenner, N., Freeman, C., Gough, R., Jones, T. G., and Lebron, I.:  
853 UV-visible absorbance spectroscopy as a proxy for peatland dissolved organic carbon  
854 (DOC) quantity and quality: considerations on wavelength and absorbance degradation,  
855 *Environmental Science: Processes and Impacts*, 10–12, doi:10.1039/c4em00108g, 2014.
- 856 Pickard, A. E., Heal, K. V., McLeod, A. R., and Dinsmore, K. J.: Temporal changes in  
857 photoreactivity of dissolved organic carbon and implications for aquatic carbon fluxes from  
858 peatlands, *Biogeosciences*, 14, 1793–1809, <https://doi.org/10.5194/bg-14-1793-2017>, 2017.
- 859 Pokrovsky, O. S., Dupré, B., and Schott, J.: Fe-Al-organic colloids control the speciation of trace  
860 elements in peat soil solutions: results of ultrafiltration and dialysis, *Aquatic Geochem.*, 11,  
861 241–278, 2005.
- 862 Pokrovsky, O. S., Viers, J., Shirokova, L. S., Shevchenko, V. P., Filipov, A. S., and Dupré, B.:  
863 Dissolved, suspended, and colloidal fluxes of organic carbon, major and trace elements in  
864 Severnaya Dvina River and its tributary, *Chem. Geol.*, 273, 136–149, 2010.
- 865 Pokrovsky, O. S., Shirokova, L. S., Zabelina, S. A., Vorobieva, T. Ya., Moreva, O. Yu., Klimov,  
866 S. I., Chupakov, A. V., Shorina, N. V., Kokryatskaya, N. M., Audry, S., Viers, J., Zoutien,  
867 C., and Freydier, R.: Size fractionation of trace elements in a seasonally stratified boreal  
868 lakes: Control of organic matter and iron colloids, *Aquat. Geochem.*, 18, 115–139, 2012.
- 869 Pokrovsky, O. S., Manasypov, R. M., Loiko, S. V., and Shirokova, L. S.: Organic and organo-  
870 mineral colloids of discontinuous permafrost zone, *Geochim. Cosmochim. Ac.*, 188, 1–20,  
871 2016.
- 872 Porcal, P., Dillon, P. J., and Molot, L. A.: Photochemical production and decomposition of  
873 particulate organic carbon in a freshwater stream, *Aquat. Sci.*, 75, 469–482, 2013.
- 874 Porcal, P., Dillon, P. J., and Molot, L. A.: Interaction of extrinsic chemical factors affecting  
875 photodegradation of dissolved organic matter in aquatic ecosystems, *Photochem. Photobiol.  
876 Sci.*, 13, 799–812, 2014.
- 877 Porcal, P., Dillon, P. J., and Molot, L. A.: Temperature dependence of photodegradation of  
878 dissolved organic matter to dissolved inorganic carbon and particulate organic carbon, *Plos  
879 ONE*, 10(6), e0128884, DOI:10.1371/journal.pone.0128884, 2015.
- 880 Prijac, A., Gandois, L., Jeanneau, L., Taillardat, P., and Garneau, M.: Dissolved organic matter  
881 concentration and composition discontinuity at the peat–pool interface in a boreal peatland,  
882 *Biogeosciences*, 19, 4571–4588, <https://doi.org/10.5194/bg-19-4571-2022>, 2022.
- 883 Raudina, T. V., Loiko, S. V., Lim, A., Manasypov, R. M., Shirokova, L. S., Istigecev, G. I.,  
884 Kuzmina, D. M., Kulizhsky, S. P., Vorobyev, S. N., and Pokrovsky, O. S.: Permafrost thaw



- 885 and climate warming may decrease the CO<sub>2</sub>, carbon, and metal concentration in peat soil  
886 waters of the Western Siberia Lowland, *Sci. Total Environ.*, 634, 1004-1023, 2018.
- 887 Raudina, T. V., Loiko, S., Kuzmina, D. M., Shirokova, L. S., Kulizhsky, S. P., Golovatskaya, E.  
888 A., and Pokrovsky, O. S.: Colloidal organic carbon and trace elements in peat porewaters  
889 across a permafrost gradient in Western Siberia, *Geoderma* 390, Art No 114971,  
890 <https://doi.org/10.1016/j.geoderma.2021.114971>, 2021.
- 891 Raudina, T. V., Smirnov, S. V., Luschaeva, I. V., Kulizhskiy, S. P., Golovatskaya, E. A.,  
892 Shirokova, L.S., and Pokrovsky, O. S.: Seasonal and spatial variations of dissolved organic  
893 matter biodegradation along the aquatic continuum in the southern taiga bog complex,  
894 Western Siberia. *Water (MDPI)*, 14, Art No 3969. <https://doi.org/10.3390/w1423396>, 2022.
- 895 Roehm, C. L., Giesler, R., Karlsson, J.: Bioavailability of terrestrial organic carbon to lake  
896 bacteria: The case of a degrading subarctic permafrost mire complex, *J. Geophys. Res.*, 114,  
897 G03006, doi: 10.1029/2008JG000863, 2009.
- 898 Rosset, T., Binet, S., Rigal, F., and Gandois, L.: Peatland dissolved organic carbon export to  
899 surface waters: Global significance and effects of anthropogenic disturbance, *Geophysical*  
900 *Res. Lett.*, 49, e2021GL096616. <https://doi.org/10.1029/2021GL096616>, 2022.
- 901 Selvam, B. P., Lapierre, J.-F., Guillemette, F., Voigt, C., Lamprecht, R. E., Biasi, C., Christensen,  
902 T. R., Martikainen P. J., and Berggren, M.: Degradation potentials of dissolved organic  
903 carbon (DOC) from thawed permafrost peat, *Scientific Reports*, 7, Art No 45811, doi:  
904 10.1038/srep45811, 2016.
- 905 Serikova, S., Pokrovsky, O. S., Ala-aho, P., Kazantsev, V., Kirpotin, S. N. Kopysov, S. G.,  
906 Krickov, I. V., Laudon, H., Manasypov, R. M., Shirokova, L. S., Sousby, C., Tetzlaff, D.,  
907 and Karlsson, J.: High riverine CO<sub>2</sub> emissions at the permafrost boundary of Western  
908 Siberia. *Nature Geoscience*, 11, 825-829, 2018.
- 909 Serikova, S., Pokrovsky, O. S., Laudon, H., Krickov, I. V., Lim, A. G., Manasypov, R. M., and  
910 Karlsson, J.: C emissions from lakes across permafrost gradient of Western Siberia, *Nature*  
911 *Comm.* 10, Art No 1552, <https://doi.org/10.1038/s41467-019-09592-1>, 2019.
- 912 Shirokova, L. S., Bredoire, R., Rolls, J. L., and Pokrovsky, O. S.: Moss and peat leachate  
913 degradability by heterotrophic bacteria: fate of organic carbon and trace metals,  
914 *Geomicrobiol. J.*, 34(8), 641-655, 2017a.
- 915 Shirokova, L. S., Chupakova, A. A., Chupakov, A. V., and Pokrovsky, O.S.: Transformation of  
916 dissolved organic matter and related trace elements in the mouth zone of the largest  
917 European Arctic river: experimental modeling, *Inland Waters*, 7(3), 272-282, 2017b.
- 918 Shirokova, L. S., Chupakov, A. V., Zabelina, S. A., Neverova, N. V., Payandi-Rolland, D.,  
919 Causseraund, C., Karlsson, J., and Pokrovsky, O. S.: Humic surface waters of frozen peat  
920 bogs (permafrost zone) are highly resistant to bio- and photodegradation, *Biogeosciences*,  
921 16, 2511–2526, 2019.
- 922 Shirokova, L. S., Chupakov, A. V., Ivanova, I. S., Moreva, O. Y., Zabelina, S. A., Shutskiy, N.  
923 A., Loiko S. V., Pokrovsky, O. S. Lichen, moss and peat control of C, nutrient and trace  
924 metal regime in lakes of permafrost peatlands. *Science Total Environ.*, 782, Art No 146737,  
925 <https://doi.org/10.1016/j.scitotenv.2021.146737>, 2021.
- 926 Spencer, R. G. M., Mann, P. J., Dittmar, T., Eglinton, T. I., McIntyre, C., Holmes, R. M., Zimov,  
927 N., Stubbins, A.: Detecting the signature of permafrost thaw in Arctic rivers, *Geophys. Res.*  
928 *Lett.*, 42, 2830-2835, 2015.
- 929 Stubbins, A., Spencer, R.G., Chen, H., Hatcher, P.G., Mopper, K.W., Hernes, P.J., Mwamba,  
930 V., Mangangu, A.M., Wabakanghanzi, J.N., and Six, J.: Illuminated darkness: Molecular  
931 signatures of Congo River dissolved organic matter and its photochemical alteration as

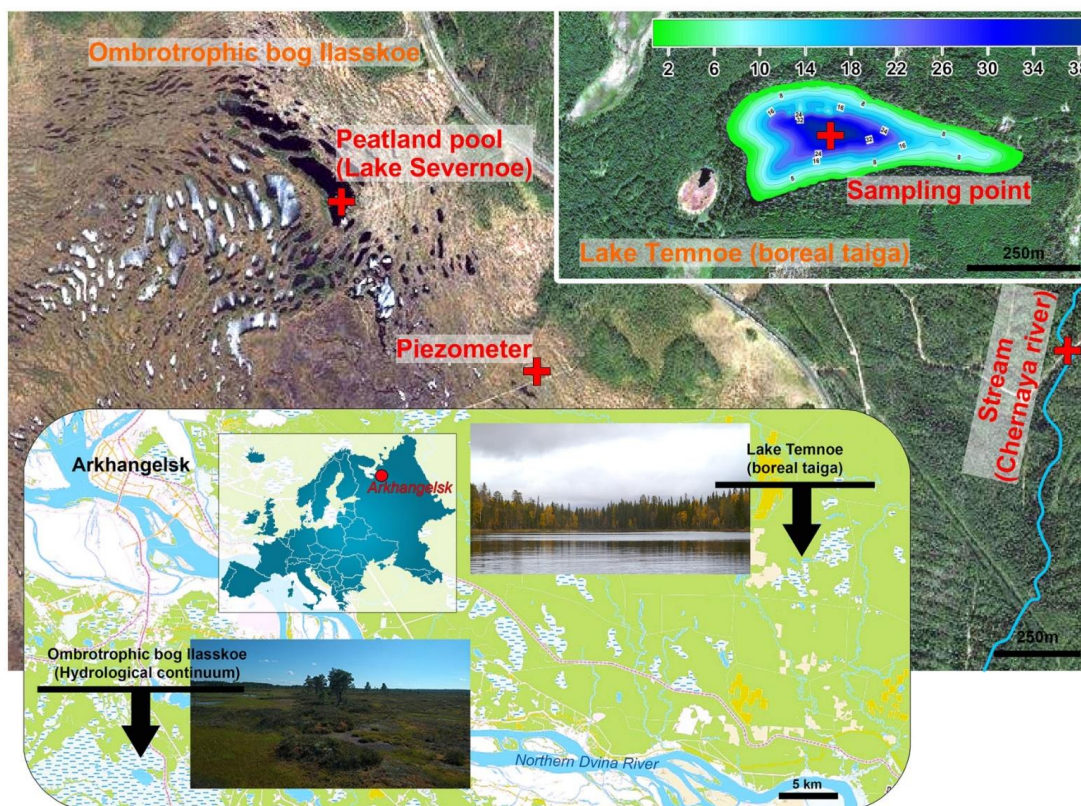




- 932 revealed by ultrahigh precision mass spectrometry. *Limnol. Oceanogr.*, 55(4), 1467-1477,  
933 10.4319/lo.2010.55.4.1467, 2010.
- 934 Stutter, M. I., Richards, S., and Dawson, J. J. C.: Biodegradability of natural dissolved organic  
935 matter collected from a UK moorland stream, *Water Res.*, 47(3), 1169-1180, 2013.
- 936 Sulzberger, B., Austin, A. T., Cory, R. M., Zepp, R. G., and Paul, N. D.: Solar UV radiation in  
937 a changing world: roles of cryosphere-land-water-atmosphere interfaces in global  
938 biogeochemical cycles, *Photochem. Photobiol. Sci.*, doi: 10.1039/c8pp90063a, 2019.
- 939 Taillardat, P., Bodmer, P., Deblois, C. P., Ponçot, A., Prijac, A., Riahi, K., et al. : Carbon  
940 dioxide and methane dynamics in a peatland headwater stream: Origins, processes and  
941 implications, *J. Geophysical Res.: Biogeosciences*, 127, e2022JG006855.  
942 <https://doi.org/10.1029/2022JG006855>, 2022.
- 943 Textor, S. R., Guillemette, F., Zito, P. A., Spencer, R. G. M.: An assessment of dissolved  
944 organic carbon biodegradability and priming in blackwater systems, *J. Geophys. Res.*  
945 *Biogeosciences*, 123(9), 2998-3015, 2018.
- 946 Tranvik, L. J., Downing, J. A., Cotner, J. B., Loiselle, S. A., Striegl, R. G., Ballatore, T. J.,  
947 Dillon, P., Finlay, K., Fortino, K., Knoll, L. B., Kortelainen, P. L., Kutser, T., Larsen, S.,  
948 Laurion, I., Leech, D. M., McCallister, S. L., McKnight, D. M., Melack, J. M., Overholt,  
949 E., Porter, J. A., Prairie, Y., Renwick, W. H., Roland, F., Sherman, B. S., Schindler, D. W.,  
950 Sobek, S., Tremblay, A., Vanni, M. J., Verschoor, A. M., von Wachenfeldt, E., and  
951 Weyhenmeyer, G. A.: Lakes and reservoirs as regulators of carbon cycling and climate,  
952 *Limnol. Oceanogr.*, 54, 2298-2314, 2009.
- 953 Vachon, D., Lapierre, J., and del Giorgio, P. A.: Seasonality of photochemical dissolved  
954 organic carbon mineralization and its relative contribution to pelagic CO<sub>2</sub> production in  
955 northern lakes, *J. Geophys. Res.-Biogeo.*, 121, 864-878,  
956 <https://doi.org/10.1002/2015JG003244>, 2016.
- 957 Vachon, D., Solomon, C. T., and del Giorgio, P. A.: Reconstructing the seasonal dynamics and  
958 relative contribution of the major processes sustaining CO<sub>2</sub> emissions in northern lakes,  
959 *Limnol. Oceanogr.*, 62, 706-722, <https://doi.org/10.1002/lno.10454>, 2017.
- 960 Vähätalo, A. V., Salonen, K., Münster, U., Järvinen, M., and Wetzel, R. G.: Photochemical  
961 transformation of allochthonous organic matter provides bioavailable nutrients in a humic  
962 lake, *Acta Hydrobiol.*, 156, 287-314, 2003.
- 963 Vähätalo, A. V. and Wetzel, R.G.: Photochemical and microbial decomposition of chromophoric  
964 dissolved organic matter during long (months-years) exposures, *Mar. Chem.*, 89, 313-326,  
965 2004.
- 966 Vasyukova, E., Pokrovsky, O. S., Viers, J., Oliva, P., Dupré, B., Martin, F., and Candaudap, F.:  
967 Trace elements in organic- and iron-rich surficial fluids of boreal zone: Assessing colloidal  
968 forms via dialysis and ultrafiltration, *Geochim. Cosmochim. Acta*, 74, 449-468, 2010.
- 969 Vonk, J. E., Tank, S. E., Mann, P. J., Spencer, R. G. M., Treat, C. C., Striegl, R. G., Abbott,  
970 B. W., and Wickland K. P.: Biodegradability of dissolved organic carbon in permafrost  
971 soils and aquatic systems: a meta-analysis, *Biogeosciences*, 12, 6915-6930, 2015.
- 972 Ward, C. P., Nalven, S. G., Crump, B. C., Kling, G. W., and Cory, R. M.: Photochemical  
973 alteration of organic carbon draining permafrost soils shifts microbial metabolic pathways  
974 and stimulates respiration, *Nature Comm.*, 8, Art No 772, 2017.
- 975 Wauthy, M., Rautio, M., Christoffersen, K. S., Forsstrom, L., Laurion, I., Mariash, H. L.,  
976 Peura, S., Vincent, W. F.: Increasing dominance of terrigenous organic matter in  
977 circumpolar freshwaters due to permafrost thaw, *Limnol. Oceanogr. Lett.*, 3, 2018, 186-  
978 198, 2012.
- 979 Weishaar, J. L., Aiken, G. R., Bergamaschi, B. A., Fram, M. S., Fujii, R., and Mopper, K.:  
980 Evaluation of specific ultraviolet absorbance as an indicator of the chemical composition



981 and reactivity of dissolved organic carbon, *Environ. Sci. Technol.*, 37, 4702–4708, 2003.  
982 Wickland, K. P., Aiken G. R., Butler K., Dornblaser M. M., Spencer R. G. M., and Striegl R.  
983 G.: Biodegradability of dissolved organic carbon in the Yukon River and its tributaries:  
984 seasonality and importance of inorganic nitrogen. *Glob Biogeochem Cycle* 26,  
985 2012gb004342, 2012.  
986 Wilske, C., Herzprung, P., Lechtenfeld, O.J., Kamjunke, N., and von Tümpling, W.:  
987 Photochemically induced changes of dissolved organic matter in a humic-rich and forested  
988 stream, *Water*, 12, 331. <https://doi.org/10.3390/w12020331>, 2020.  
989 Winter, A. R., Fish, T. A. E., Playle, R. C., Smith, D. S., and Curtis, P. J.: Photodegradation of  
990 natural organic matter from diverse freshwater sources, *Aquat. Toxicol.*, 84, 215-222,  
991 2007.  
992 Zabelina, S.A., Shirokova, L.S., Klimov, S.I., Chupakov, A.V., Lim, A.G., Polishchuk, Y.M.,  
993 Polishchuk, V.Y., Bogdanov, A.N., Muratov, I.N., Guerin, F., Karlsson, J., and Pokrovsky,  
994 O.S.: Carbon emission from thermokarst lakes in NE European tundra, *Limnol. Oceanogr.*,  
995 66, S216-S230. <https://doi.org/10.1002/lno.11560>, 2021.  
996  
997  
998  
999



1000

1001

1002

1003

1004 **Fig. 1.** Geographical location of studied hydrological continuum for Ilasskoe Bog waters and  
1005 deep stratified Lake Temnoe in the boreal forest. Photo and map credits of Chupakov A.V.

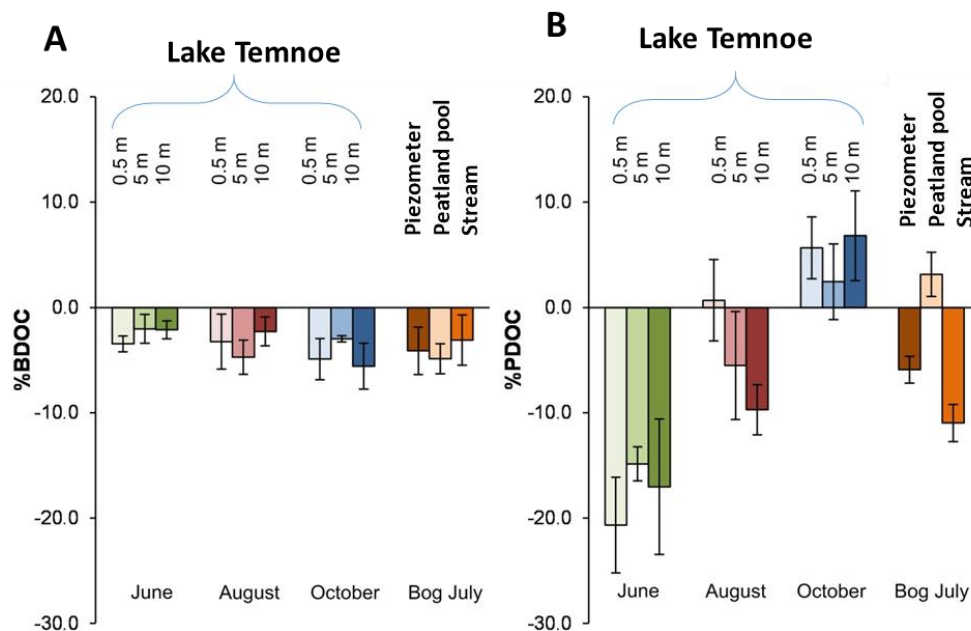
1006

1007

1008

1009

1010



1011

1012

1013

1014

1015 **Fig. 2.** Percentage of bio- (A) and photo- (B) degradable DOC presented as relative decrease in  
1016 DOC concentration between the initial and final value for the Temnoe Lake (June, August and  
1017 October) and Ilasskoe Bog surface waters (July). Error bars are 1 s.d. of duplicates relative to  
1018 the control (see Eqn. 1-2 in the text). Positive values signify nil photodegradation (experimental  
1019 artifacts of DOC production).

1020

1021

1022

1023

1024

1025

1026

1027

1028

1029

1030

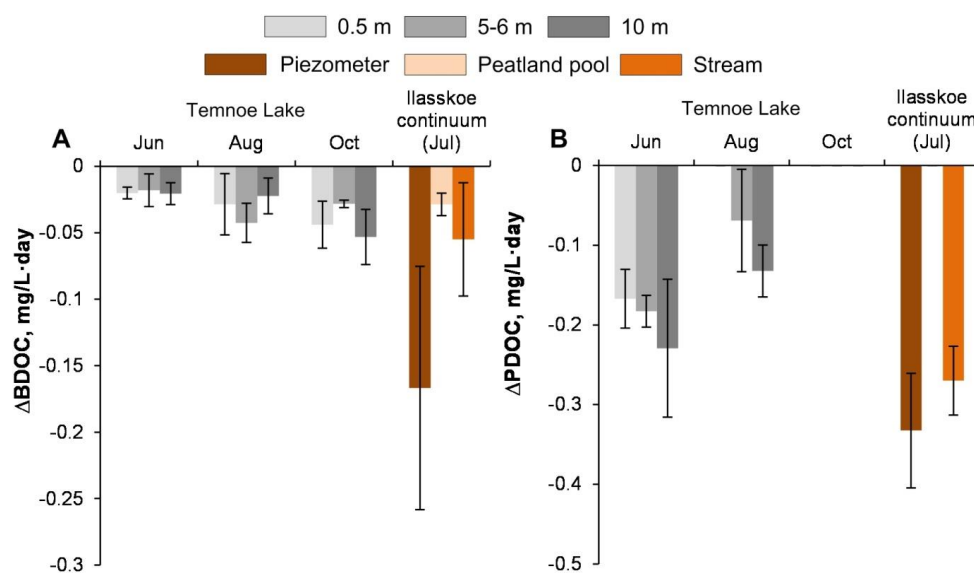
1031



1032

1033

1034



1035

1036

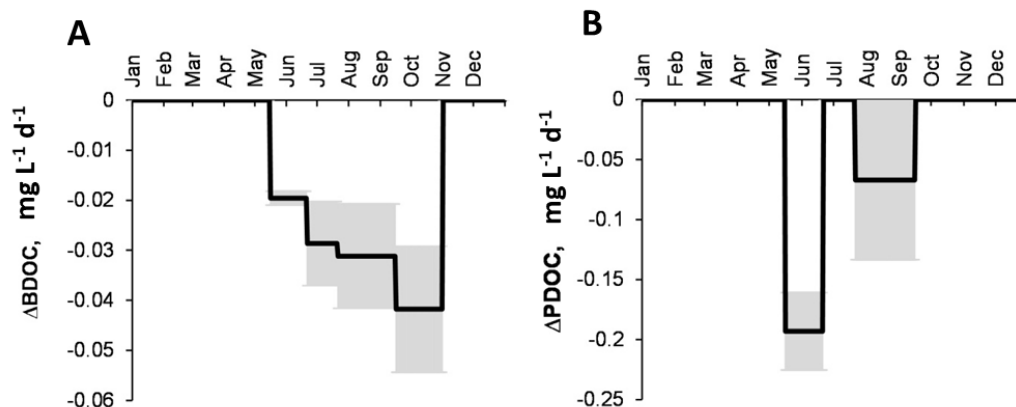
1037 **Fig. 3.** Rates of DOC bio- (A) and photo- (B) degradation. The values are negative because  
1038 they represent a decrease in DOC concentration over the course of the experiment.

1039

1040

1041

1042



1043

1044

1045

1046 **Fig. 4.** Integral rates of bio- ( $\Delta\text{BDOC}$ , **A**) and photo- ( $\Delta\text{PDOC}$ , **B**) degradation in the 0-10 m  
1047 layer of Lake Temnoe across the entire open-water period (May to October). Rate values are  
1048 negative because they signify a decrease in DOC concentration. Uncertainties are represented  
1049 by gray shaded rectangles.

1050

1051

1052

1053

1054

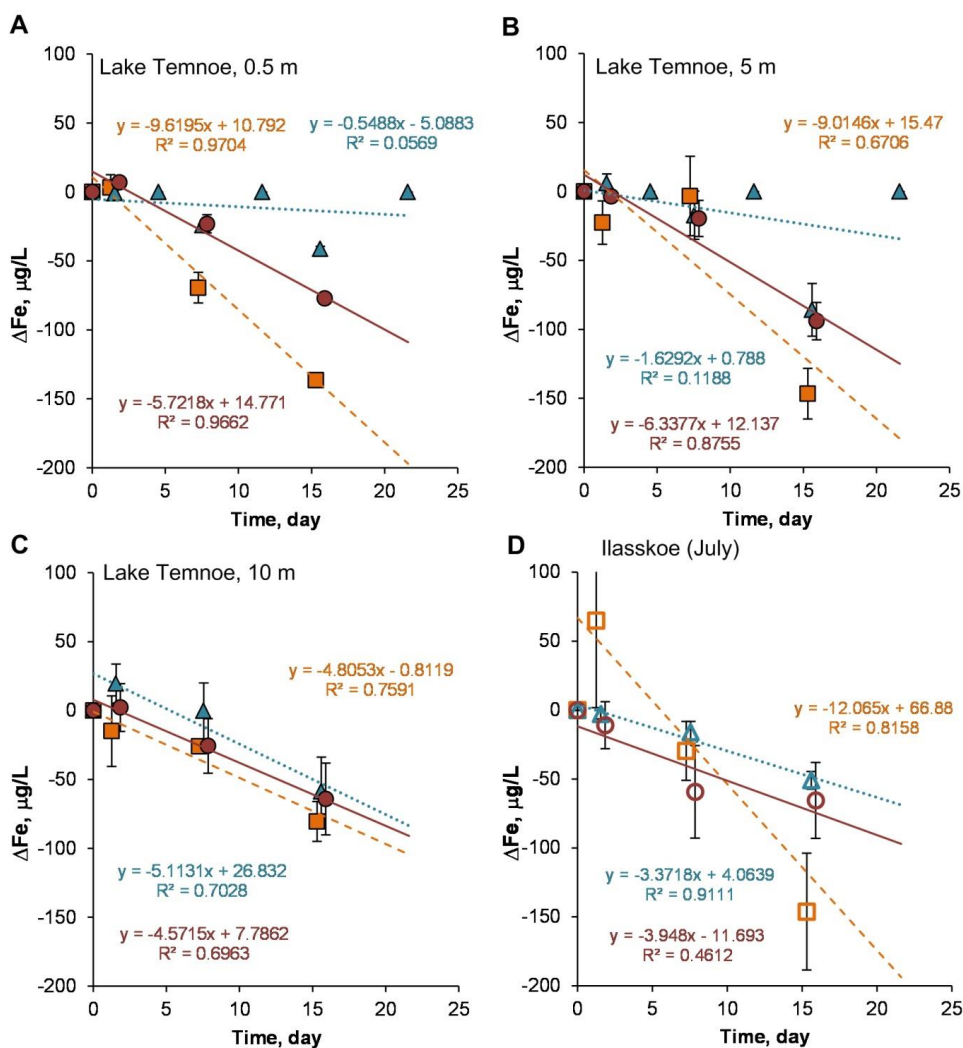
1055

1056

1057

1058

1059



1060    ■ June    ▲ August    ● October    □ Piezometer    ▲ Peatland pool    ○ Stream

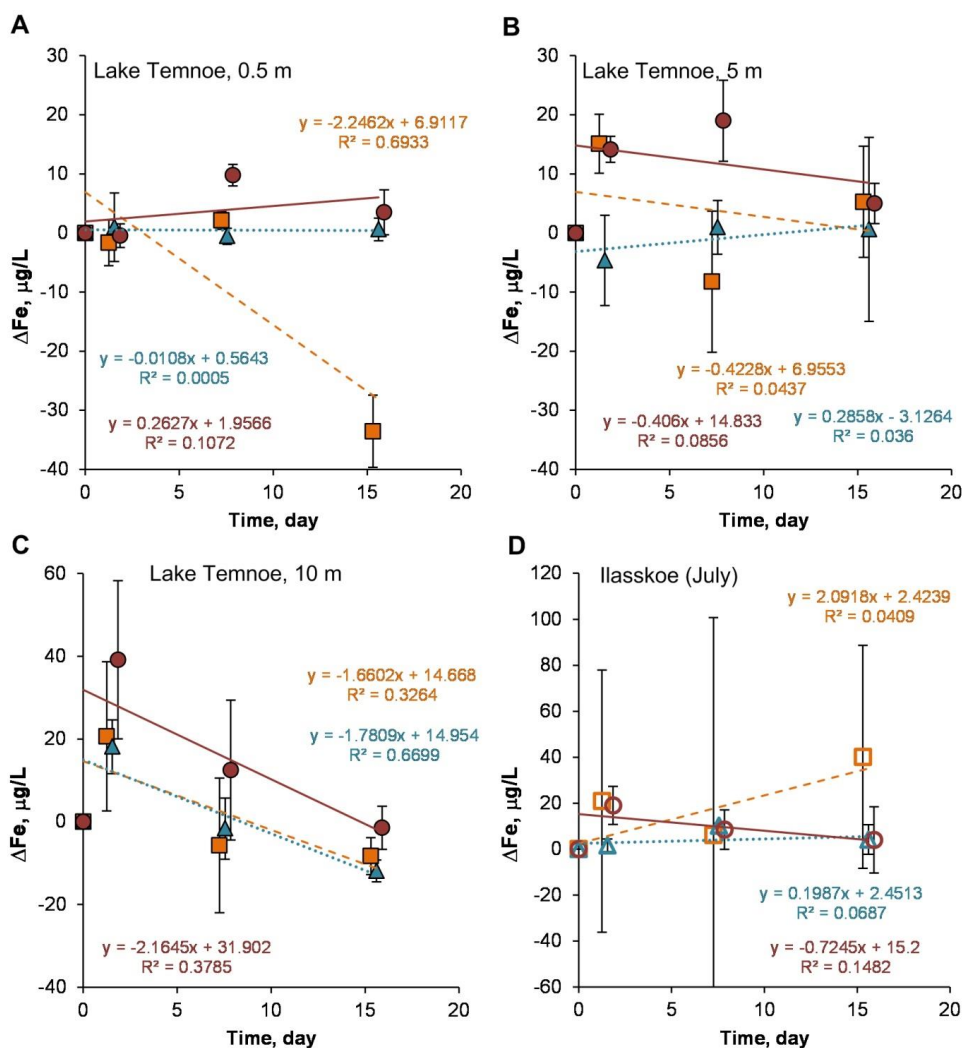
1061

1062 **Fig. 5.** Change in Fe concentration (relative to control) over time in biodegradation  
 1063 experiments. Error bars are 1 s.d. of duplicates. Temnoe Lake 0.5 m (A), 5 m (B) and 10 m (C)  
 1064 in June (squares), August (triangles) and October (circles). Ilasskoe Bog continuum in July (D)  
 1065 including piezometer (squares), Severnoe peatland pool (triangles) and stream Chernyi  
 1066 (circles).

1067

1068

1069



1070 ■ June ▲ August ● October □ Piezometer △ Peatland pool ○ Stream

1071

1072

1073

**Fig. 6.** Change in Fe concentration (relative to the control) over time in photo-degradation experiments. The error bars are 1 s.d. of duplicates. Lake Temnoe 0.5 m (A), 5 m (B) and 10 m (C) in June (squares), August (triangles) and October (circles). Ilaskoe continuum in July (D) includes piezometer (squares), peatland pool Severnoe (triangles) and stream Chernyi (circles)

1074

1075

1076

1077

1078

1079

1080

1081





1082 **Table 1.** Landscape setting, hydrochemical characteristics and CO<sub>2</sub> concentration and emission  
 1083 flux of studied waters. S.C. is specific conductivity and EB and OB is eutrophic and  
 1084 oligotrophic bacteria count, respectively.

1085 **1A.** Ilaskoe bog continuum in July.

1086

	Piezometer	Lake Severnoe	Stream Chernyi
<b>GPS coordinates</b>	N64.328694° E40.612556°	N64.334361° E40.609667°	N64.330982° E40.653352°
<b>Description</b>	Shallow groundwater	Peatland pool	Outlet stream
<b>T, °C</b>	11.4	19.4	13
<b>O<sub>2</sub>, mg/L</b>	0.6	8.6	7.5
<b>pH</b>	3.9	4.0	5.7
<b>S.C., μS cm<sup>-1</sup></b>	46	17	26
<b>DOC, mg L<sup>-1</sup></b>	87.6	12.7	38.4
<b>DIC, mg L<sup>-1</sup></b>	0.32	0.40	0.38
<b>SUVA<sub>254</sub></b>	4.13	3.80	4.85
<b>P-PO<sub>4</sub>, μg L<sup>-1</sup></b>	8.6	3.0	1.7
<b>P<sub>total</sub>, μg L<sup>-1</sup></b>	153	10	20
<b>N-NO<sub>3</sub>, μg L<sup>-1</sup></b>	111	70	98
<b>N-NH<sub>4</sub>, μg L<sup>-1</sup></b>	85.4	16.1	12.6
<b>N<sub>total</sub>, μg L<sup>-1</sup></b>	1180	222	399
<b>Si, μg L<sup>-1</sup></b>	1808	47	2076
<b>CO<sub>2</sub>, μmol/L</b>	3360	55	318
<b>CO<sub>2</sub> flux, mmol m<sup>-2</sup> d<sup>-1</sup></b>	1600	22	151
<b>EB, CFU mL<sup>-1</sup></b>	49360	56600	9000
<b>OB, CFU mL<sup>-1</sup></b>	54560	37900	21600

1087

1088 **1B.** Lake Temnoe across seasons and depths.

1089

1090

Month	Jun	Jun	Jun	Aug	Aug	Aug	Oct	Oct	Oct
	0.5	5	10	0.5	5	10	0.5	6	10
<b>GPS</b>	N64.47683°			E041.74533°					
<b>Description</b>	Lake in the northern taiga								
<b>T, °C</b>	12.7	4,9	4,5	18.4	5.5	4.3	9.0	5.8	4.4
<b>O<sub>2</sub>, mg/L</b>	8,45	4,8	4,5	7.78	4.93	2.63	8.90	4.46	2.14
<b>pH</b>	5.2	5.2	5.3	6.0	5.5	5.7	5.2	5.2	5.1
<b>S.C., μS cm<sup>-1</sup></b>	17	17	19	17	17	19	18	18	20
<b>DOC, mg L<sup>-1</sup></b>	12.6	19.2	21	19	19.5	21.2	19.4	20.6	20.6
<b>DIC, mg L<sup>-1</sup></b>	0.55	0.53	0.49	0.70	0.71	0.66	0.67	0.67	0.64
<b>SUVA<sub>254</sub></b>	4.6	4.7	4.6	4.2	4.5	4.5	4.3	4.3	4.7
<b>P-PO<sub>4</sub>, μg L<sup>-1</sup></b>	2.9	3.3	6.4	0.9	3.6	9.4	3.8	4.6	4.2
<b>P<sub>total</sub>, μg L<sup>-1</sup></b>	19	17	19	20	16	20	18	19	20
<b>N-NO<sub>3</sub>, μg L<sup>-1</sup></b>	119	150	137	86	152	254	88	85	100
<b>N-NH<sub>4</sub>, μg L<sup>-1</sup></b>	7.1	8.0	10.0	9.1	17.5	13.8	16.4	14.1	15.5
<b>N<sub>total</sub>, μg L<sup>-1</sup></b>	305	420	408	355	315	337	425	416	396
<b>Si, μg L<sup>-1</sup></b>	1940	2268	2354	1183	2208	2714	2269	2380	2380
<b>CO<sub>2</sub>, μmol/L</b>	99	309	329	110	256	337	223	232	253
<b>CO<sub>2</sub> flux, mmol m<sup>-2</sup> d<sup>-1</sup></b>	32	-	-	46	-	-	71	-	-
<b>EB, CFU mL<sup>-1</sup></b>	-	36	50	259	92	270	780	220	105
<b>OB, CFU mL<sup>-1</sup></b>	50	570	420	-	190	-	680	150	66

1091



**Table 2.** The % bio- and photodegradable solutes (mean  $\pm$  s.d.) whose relative change (concentration decrease) in the course of experiment was superior to that of SD. Prefix  $\Delta B$  and  $\Delta P$  represents the effect of bio- and photodegradation, respectively. Duration of biodegradation and photodegradation is  $21.6 \pm 0.1$  and  $15.6 \pm 0.1$  days, respectively.  $W$  represents the probability of measurable effect, significantly different from changes in the control reactors. Only the components with  $W \geq 33\%$  are presented. Tennoe Lake is deep stratified lake in the forest. Peizometer, peatland pool and outlet stream represent the hydrological continuum of the Illasskoe Bog.

Index	Tennoe Lake 5 m (Jun)		Tennoe Lake 10 m (Jun)		Tennoe Lake 0.5 m (Aug)		Tennoe Lake 5 m (Aug)		Tennoe Lake 10 m (Aug)		Tennoe Lake 0.5 m (Oct)		Tennoe Lake 6 m (Oct)		Tennoe Lake 10 m (Oct)		Piezometer (Jul)	Peatland pool (Jul)	Outlet stream (Jul)
	17	17	19	17	17	17	19	17	19	17	19	18	18	18	18	20	46	17	26
$\bar{x}$ , $\mu S/cm$	17	17	19	17	17	17	19	17	19	17	19	18	18	18	20	46	17	26	
$\Delta B(\bar{x} \pm SD)$	-24 $\pm$ 4	-26 $\pm$ 7	-30 $\pm$ 5	-23 $\pm$ 3	-27 $\pm$ 3	-23 $\pm$ 3	-24 $\pm$ 7	-23 $\pm$ 4	-24 $\pm$ 7	-23 $\pm$ 4	-23 $\pm$ 4	-23 $\pm$ 4	-23 $\pm$ 4	-23 $\pm$ 4	-17 $\pm$ 5	0	-18 $\pm$ 10	-29 $\pm$ 4	
DOC, mg/L	12.6	19.2	21.0	19.0	19.5	19.5	21.2	19.4	20.6	20.6	20.6	20.6	20.6	20.6	20.6	87.6	12.7	38.4	
$\Delta B(DOC \pm SD)$	3.4 $\pm$ 0.8	2.0 $\pm$ 1.4	2.1 $\pm$ 0.8	3.2 $\pm$ 2.6	4.7 $\pm$ 1.6	2.3 $\pm$ 1.4	4.9 $\pm$ 2.0	3.0 $\pm$ 0.3	3.0 $\pm$ 0.3	3.0 $\pm$ 0.3	3.0 $\pm$ 0.3	3.0 $\pm$ 0.3	3.0 $\pm$ 0.3	3.0 $\pm$ 0.3	5.6 $\pm$ 2.2	4.1 $\pm$ 2.3	4.9 $\pm$ 1.4	3.1 $\pm$ 2.4	
$\Delta P(DOC \pm SD)$	20.7 $\pm$ 4.6	14.9 $\pm$ 1.6	17.0 $\pm$ 6.4	0	5.5 $\pm$ 5.1	9.7 $\pm$ 2.4	0	0	0	0	0	0	0	0	0	5.9 $\pm$ 1.3	0	11.0 $\pm$ 1.8	
Al, $\mu g/L$	275	298	329	254	296	254	275	275	288	288	288	288	288	288	323	276	59	388	
$\Delta B(Al \pm SD)$	3.5 $\pm$ 1.4	1.8 $\pm$ 0.9	0	2.0 $\pm$ 1.3	0	1.4 $\pm$ 1.5	2.0 $\pm$ 1.9	0	0	0	0	0	0	0	0	0.9 $\pm$ 2.2	0	1.3 $\pm$ 1.8	
$\Delta P(Al \pm SD)$	1.9 $\pm$ 1.1	2.7 $\pm$ 0.9	3.6 $\pm$ 1.3	0	2.5 $\pm$ 1.3	1.7 $\pm$ 2.0	0.7 $\pm$ 0.9	0	0	0	0	0	0	0	0	0	0	0.8 $\pm$ 0.9	
Ti, $\mu g/L$	1.5	2.1	2.6	1.1	2.0	2.6	1.7	1.9	1.9	1.9	1.9	1.9	1.9	1.9	2.5	3.7	0.6	5.0	
$\Delta B(Ti \pm SD)$	-9.2 $\pm$ 1.6	-9.9 $\pm$ 7.4	-2.6 $\pm$ 2.7	-4.8 $\pm$ 3.4	-1.8 $\pm$ 2.7	0	-3.6 $\pm$ 1.7	-1.0 $\pm$ 3.1	-1.0 $\pm$ 3.1	-1.0 $\pm$ 3.1	-1.0 $\pm$ 3.1	-1.0 $\pm$ 3.1	-1.0 $\pm$ 3.1	-1.0 $\pm$ 3.1	-1.0 $\pm$ 3.9	-2.3 $\pm$ 3.6	-2.2 $\pm$ 1.7	-1.4 $\pm$ 2.2	
$\Delta P(Ti \pm SD)$	-0.1 $\pm$ 3	-3 $\pm$ 3	-8 $\pm$ 3	0 $\pm$ 0	-9 $\pm$ 1	-3 $\pm$ 2	-2 $\pm$ 4	0	0	0	0	0	0	0	0	0	0	-3.3 $\pm$ 0.5	
V, $\mu g/L$	0.5	0.6	0.7	0.4	0.5	0.7	0.4	0.5	0.5	0.5	0.5	0.5	0.5	0.5	0.7	1.1	0.5	1.3	
$\Delta B(V \pm SD)$	-8.3 $\pm$ 16.2	-5.4 $\pm$ 3.2	-4.9 $\pm$ 2.3	-6.8 $\pm$ 7.5	-10.0 $\pm$ 4.6	-1.7 $\pm$ 1.6	-14.7 $\pm$ 11	-13.9 $\pm$ 4.3	-13.9 $\pm$ 4.3	-13.9 $\pm$ 4.3	-13.9 $\pm$ 4.3	-13.9 $\pm$ 4.3	-13.9 $\pm$ 4.3	-13.9 $\pm$ 4.3	-16.1 $\pm$ 1.7	-3.2 $\pm$ 2.6	-0.2 $\pm$ 3.4	-17.9 $\pm$ 5.0	
Mn, $\mu g/L$	39	55	79	17	48	93	30	47	47	47	47	47	47	47	105	78	9	47	
$\Delta B(Mn \pm SD)$	0	0	-0.3 $\pm$ 2.2	-31.8 $\pm$ 1.3	-3.2 $\pm$ 1.6	-0.6 $\pm$ 2.2	-4.8 $\pm$ 2.2	-3.2 $\pm$ 1.7	-3.2 $\pm$ 1.7	-3.2 $\pm$ 1.7	-3.2 $\pm$ 1.7	-3.2 $\pm$ 1.7	-3.2 $\pm$ 1.7	-3.2 $\pm$ 1.7	-0.4 $\pm$ 0.1	0	0	-1.6 $\pm$ 2.8	
Fe, $\mu g/L$	358	527	710	165	460	795	317	448	448	448	448	448	448	448	820	4402	157	1006	
$\Delta B(Fe \pm SD)$	-18.1 $\pm$ 2.5	-9.1 $\pm$ 2.6	-5.4 $\pm$ 1.6	-13.5 $\pm$ 1.0	-6.3 $\pm$ 2.6	-1.4 $\pm$ 1.9	-9.5 $\pm$ 1.4	-7.8 $\pm$ 1.9	-7.8 $\pm$ 1.9	-7.8 $\pm$ 1.9	-7.8 $\pm$ 1.9	-7.8 $\pm$ 1.9	-7.8 $\pm$ 1.9	-7.8 $\pm$ 1.9	-3.3 $\pm$ 1.8	-0.8 $\pm$ 0.8	-13.6 $\pm$ 4.3	-4.5 $\pm$ 2.4	
$\Delta P(Fe \pm SD)$	-3.9 $\pm$ 0.6	-2.0 $\pm$ 1.9	-4.0 $\pm$ 1.3	0	-2.9 $\pm$ 1.5	-0.2 $\pm$ 0.6	-1.2 $\pm$ 0.4	0	0	0	0	0	0	0	0	0	0	0	



1093 **Table 2**, continued.

Index	Temnoe Lake 5 m (Jun)		Temnoe Lake 10 m (Jun)		Temnoe Lake 0.5 m (Aug)		Temnoe Lake 5 m (Aug)		Temnoe Lake 10 m (Aug)		Temnoe Lake 0.5 m (Oct)		Temnoe Lake 6 m (Oct)		Temnoe Lake 10 m (Oct)		Piezo-meter (Jul)	Peatland pool (Jul)	Outlet stream (Jul)	
	0.28	0.39	0.68	0.07	0.30	0.65	0.18	0.31	0.74	0.30	0.65	0.7	0.7	0.7	0.7	0.7				0.7
Co, µg/L	0.28	0.39	0.68	0.07	0.30	0.65	0.18	0.31	0.74	0.30	0.65	0.7	0.7	0.7	0.7	0.7	0.7	0.45	0.06	0.30
$\Delta B(Ce \pm SD)$	-2.2±5.1	-1.2±2.1	-3.7±4.6	-32.7±2.6	-8.1±5.6	-2.7±3.3	-11.0±4.4	-9.1±5.1	-1.6±0.4	0	0	0	0	0	0	0	0	0	0	-20.6±27.8
Cu, µg/L	0.5	0.6	0.7	0.6	0.6	0.7	0.7	0.7	0.5	0.8	0.8	0.8	0.8	0.8	0.8	0.8	0.8	1.5	0.3	0.8
$\Delta B(Cu \pm SD)$	0	0	0	-14.3±1.4	-6.8±4.0	-17.9±11.0	-5.3±4.8	-4.1±8.0	-1.4±12.3	0	0	0	0	0	0	0	0	0	0	-7.7±9.9
Ga, µg/L	0.017	0.022	0.026	0.012	0.016	0.023	0.017	0.015	0.024	0.016	0.023	0.017	0.015	0.024	0.016	0.024	0.016	0.126	0.016	0.066
$\Delta P(Ga \pm SD)$	-14±6	-13±5	-10±4	0	-1±8	0	-10±4	0	0	0	0	0	0	0	0	0	0	-7±5	-5±8	-6±3
Y, µg/L	0.22	0.25	0.28	0.20	0.24	0.28	0.22	0.23	0.28	0.28	0.22	0.22	0.23	0.28	0.28	0.28	0.28	0.10	0.01	0.21
$\Delta P(Y \pm SD)$	-1.3±4.6	-6.7±0.9	-5.3±2.5	0	-2.3±0.7	-1.0±1.6	-1.4±0.2	0	0	0	0	0	0	0	0	0	0	0	0	-5.8±2.7
Zr, µg/L	0.4	0.4	0.5	0.4	0.5	0.5	0.4	0.4	0.5	0.4	0.4	0.4	0.4	0.5	0.4	0.5	0.4	0.3	0.1	0.4
$\Delta P(Zr \pm SD)$	-15±4	-14±0	-13±2	-9±20	-17±1	-14±3	-4±4	0	0	0	0	0	0	0	0	0	0	0	0	-32±3
Nb, µg/L	0.016	0.020	0.025	0.012	0.020	0.024	0.017	0.018	0.025	0.024	0.017	0.018	0.018	0.025	0.025	0.025	0.025	0.033	0.005	0.042
$\Delta B(Nb \pm SD)$	-3.6±10.2	-1.7±7.0	0	-7.7±4.8	-1.1±2.6	0	-7.3±2.3	-1.5±6.3	-5.0±4.0	0	0	0	0	0	0	0	0	-2.4±1.5	0	0
$\Delta P(Nb \pm SD)$	-9±3	-8±3	-9±1	-6±23	-13±2	-10±5	-8±4	0	-3±3	0	0	0	0	0	0	0	0	0	0	-13±10
Ba, µg/L	4.8	5.1	5.8	4.6	5.0	5.7	4.9	4.8	5.6	5.7	4.9	4.8	4.8	5.6	5.6	5.6	5.6	54.4	1.5	56.8
$\Delta B(Ba \pm SD)$	-2.2±0.7	-2.8±1.7	-1.0±2.7	0	0	0	-1.9±0.5	-1.7±3.7	-5.9±1.6	0	0	0	0	0	0	0	0	0	0	-1.3±3.4
La, µg/L	0.23	0.26	0.30	0.21	0.26	0.32	0.24	0.27	0.31	0.32	0.24	0.27	0.27	0.31	0.31	0.31	0.31	0.07	0.01	0.22
$\Delta B(La \pm SD)$	-4.9±6.5	0	0	-3.9±0.9	-0.3±1.6	-2.6±1.5	-1.1±3.6	-2.4±1.2	-4.0±2.8	0	0	0	0	0	0	0	0	-0.8±10.4	-29.7±10.0	-2.0±2.8
$\Delta P(La \pm SD)$	-3.8±3.6	-1.2±5.9	-2.0±2.7	0	-3.6±1.0	-3.2±1.6	-1.8±0.9	-2.6±1.0	0	0	0	0	0	0	0	0	0	0	0	-13.5±3.0
Ce, µg/L	0.58	0.65	0.71	0.50	0.62	0.78	0.59	0.63	0.78	0.78	0.59	0.63	0.63	0.78	0.78	0.78	0.78	0.21	0.03	0.56
$\Delta B(Ce \pm SD)$	-5.2±4.2	0	0	-4.4±0.7	-0.1±1.4	-0.8±1.0	-0.9±2.9	-0.8±1.1	-2.2±2.2	0	0	0	0	0	0	0	0	0	0	-2.0±1.9
$\Delta P(Ce \pm SD)$	-4.9±1.9	-6.2±1.2	-1.1±1.7	0	-1.5±0.5	-3.2±1.7	-1.9±1.2	0	-0.047±0.46	0	0	0	0	0	0	0	0	-3.7±1.5	-2.4±1.6	-3.6±1.1

1094  
 1095  
 1096



1097 **Table 2**, continued.

Index	Temnoe Lake 0.5 m (Jun)		Temnoe Lake 5 m (Jun)		Temnoe Lake 10 m (Jun)		Temnoe Lake 0.5 m (Aug)		Temnoe Lake 10 m (Aug)		Temnoe Lake 0.5 m (Oct)		Temnoe Lake 10 m (Oct)		Piezometer (Jul)	Peatland pool (Jul)	Outlet stream (Jul)
	Value	SD	Value	SD	Value	SD	Value	SD	Value	SD	Value	SD	Value	SD	Value	Value	Value
Pr, µg/L	0.075	0.085	0.094	0.069	0.082	0.105	0.077	0.084	0.102	0.027	0.005	0.070	0.005	0.070	0.027	0.005	0.070
ΔB(Pr±SD)	-1.9±5.2	0	-4.0±1.1	0	-0.7±1.3	0	-0.9±1.6	-3.2±2.3	-3.0±1.7	-10.8±8.4	-1.7±2.3	-3.0±1.7	-10.8±8.4	-1.7±2.3	-3.0±1.7	-10.8±8.4	-1.7±2.3
ΔP(Pr±SD)	-3.0±3.9	-5.5±0.9	-0.4±2.9	13.7±20.8	0	-6.1±2.8	0	-1.3±1.8	0	-0.01±2.4	-16.9±3.0	-2.4±2.1	-0.01±2.4	-16.9±3.0	-2.4±2.1	-0.01±2.4	-16.9±3.0
Nd, µg/L	0.33	0.34	0.39	0.29	0.33	0.42	0.33	0.32	0.41	0.11	0.02	0.27	0.11	0.02	0.27	0.11	0.02
ΔP(Nd±SD)	-7.8±2.4	-4.5±2.5	-0.8±2.1	0	0	-3.8±2.5	-2.0±3.3	0	-2.5±2.8	-24.7±6.2	0	-2.5±2.8	-24.7±6.2	0	-2.5±2.8	-24.7±6.2	0
Eu, µg/L	0.015	0.017	0.016	0.012	0.016	0.020	0.014	0.018	0.021	0.011	0.001	0.017	0.011	0.001	0.017	0.011	0.001
ΔP(Eu±SD)	0	-10.9±3.3	0	0	-0.8±4.7	-3.0±4.0	0	-8.7±8.4	-6.9±4.2	-23.7±8.6	-58.2±15.2	-1.0±1.0	-23.7±8.6	-58.2±15.2	-1.0±1.0	-23.7±8.6	-58.2±15.2
Gd, µg/L	0.06	0.07	0.08	0.05	0.07	0.08	0.06	0.07	0.09	0.02	0.00	0.06	0.02	0.00	0.06	0.02	0.00
ΔP(Gd±SD)	-0.2±4.4	-6.5±2.9	-3.5±3.5	0	-6.0±3.2	-7.6±1.9	-2.3±2.0	0	-6.7±3.2	0	0	0	-6.7±3.2	0	0	0	0
Ho, µg/L	0.009	0.009	0.011	0.007	0.009	0.011	0.009	0.009	0.011	0.004	0.0004	0.009	0.004	0.0004	0.009	0.004	0.0004
ΔP(Ho±SD)	-1.9±1.5	-0.3±1.6	-4.6±6.5	0	-0.1±3.6	-3.4±3.2	-11.0±4.9	0	-21.5±11.3	-10.9±5.5	0	-21.5±11.3	-10.9±5.5	0	-21.5±11.3	-10.9±5.5	0
Er, µg/L	0.023	0.025	0.033	0.022	0.026	0.030	0.022	0.023	0.031	0.011	0.001	0.023	0.011	0.001	0.023	0.011	0.001
ΔB(Er±SD)	0	0	0	-5.2±3.0	-2.1±1.8	0	-2.1±3.5	0	-15.6±4.9	-22.9±19.5	0	-15.6±4.9	-22.9±19.5	0	-15.6±4.9	-22.9±19.5	0
Pb, µg/L	0.23	0.24	0.23	0.16	0.23	0.39	0.28	0.28	0.32	11	0.35	0.65	11	0.35	0.65	11	0.35
ΔB(Pb±SD)	0	0	0	-21.3±2.5	-2.0±7.6	-2.4±1.6	-8.2±3.3	-7.2±9.9	-0.8±2.7	0	-17.4±1.0	-8.5±10.9	0	-17.4±1.0	-8.5±10.9	0	-17.4±1.0
Th, µg/L	0.046	0.052	0.066	0.058	0.054	0.064	0.053	0.054	0.061	0.019	0.005	0.050	0.019	0.005	0.050	0.019	0.005
ΔP(Th±SD)	0	0	-11.6±2.6	-12.2±22.5	-7.8±3.2	-18.1±5.6	0	-2.0±1.9	-49.5±1.3	-10.6±0.8	0	-49.5±1.3	-10.6±0.8	0	-49.5±1.3	-10.6±0.8	0



1099  
1100  
1101  
1102  
1103

**Table 3.** Mean ( $\pm$ SD), depth-integrated rates of bio- and photodegradation ( $\text{mg C L}^{-1}\text{d}^{-1}$ )

Object	$V_{\text{Biodegradation}}$	$V_{\text{Photodegradation}}$
Lake Temnoe		
Forest Lake (Jun)	$-0.02 \pm 0.0014$	$-0.19 \pm 0.03$
Forest Lake (Aug)	$-0.031 \pm 0.010$	$-0.067 \pm 0.066$
Forest Lake (Oct)	$-0.042 \pm 0.013$	0
Illasskoe Bog continuum (July)		
Piezometer water	$-0.17 \pm 0.09$	$-0.33 \pm 0.07$
Peatland pool	$-0.029 \pm 0.008$	0
Outlet stream (Chernyi)	$-0.055 \pm 0.043$	$-0.27 \pm 0.043$

1104  
1105  
1106  
1107  
1108  
1109  
1110  
1111  
1112